Extracellular vesicles and co-isolated endogenous retroviruses from murine cancer cells differentially affect dendritic cells

Federico Cocozza, Lorena Martin-Jaular, Lien Lippens, Aurelie Di Cicco, Yago Arribas, Nicolas Ansart, Florent Dingli, Michael Richard, Louise Merle, Mabel Jouve San Roman, et al.

Extracellular vesicles and co-isolated endogenous retroviruses differently affect dendritic cells

Federico Cocozza[1,2], Lorena Martin-Jaular[1,3], Lien Lippens[4], Aurelie Di Cicco[5,6], Yago A Arribas[1], Nicolas Ansart[1], Florent Dingli[7], Michael Richard[7], Louise Merle[1], Mabel Jouve[8], Patrick Poullet[9], Damarys Loew[7], Daniel Lévy[5,6], An Hendrix[4], George Kassiotis[10], Alain Joliot[1], Mercedes Tkach[1]*, Clotilde Théry[1,3]*

[1]INSERM U932, Institut Curie Centre de Recherche, PSL Research University, F-75005, Paris, France
[2]Université de Paris, F-75006, Paris, France
[3]Institut Curie centre de recherche, CurieCoreTech Extracellular Vesicles, F-75005, Paris, France
[4]Laboratory of Experimental Cancer Research, Ghent University, Ghent, Belgium
[5]Institut Curie, PSL Research University, Sorbonne Université, CNRS UMR168, Laboratoire Physico-chimie Curie, F-75005, Paris, France
[6]Institut Curie, PSL Research University, CNRS UMR144, Cell and Tissue Imaging Facility (PICT-IBiSA), F-75005, Paris, France
[7]Institut Curie, PSL Research University, Centre de Recherche, CurieCoreTech Spectrométrie de Masse Protéomique, F-75005, Paris, France
[8]CNRS UMR3215, Institut Curie, PSL Research University, F-75005, Paris, France
[9]Institut Curie, Bioinformatics core facility (CUBIC), INSERM U900, PSL Research University, Mines Paris Tech, F-75005, Paris, France
[10]Retroviral Immunology, The Francis Crick Institute and Department of Medicine, Faculty of Medicine, Imperial College, London UK

*co-last authors.
Correspondence to: clotilde.thery@curie.fr. ORCID 0000-0001-8294-6884
mercedes.tkach@gmail.com. ORCID 0000-0002-8011-9444

Total character count: 91215 (w space, w/o figure legends)

ABSTRACT

Cells secrete extracellular vesicles (EVs) and non-vesicular extracellular (nano)particles (NVEPs or ENPs) that may play a role in intercellular communication. Tumor-derived EVs have been proposed to induce immune priming of antigen presenting cells, or to be immuno-suppressive agents. We suspect that such disparate functions are due to variable compositions in EV subtypes and ENPs. We aimed to characterize the array of secreted EVs and ENPs of murine tumor cell lines. Unexpectedly, we identified virus-like particles (VLPs) from endogenous murine leukemia virus in preparations of EVs produced by many tumor cells. We established a protocol to separate small (s)EVs from VLPs and ENPs. We compared their protein composition and analyzed their functional interaction with target dendritic cells (DCs). ENPs were poorly captured and did not affect DCs. sEVs specifically induced DC death. A mixed large EV/VLP preparation was most efficient to induce DC maturation and antigen presentation. Our results call for systematic re-evaluation of the respective proportions and functions of non-viral EVs and VLPs produced by tumors and their contribution to tumor progression.

Keywords:
antigen presenting cells / exosomes / extracellular vesicles / non vesicular extracellular particles / retrovirus / tumors.

Figures to be downloaded:
http://xfer.curie.fr/get/qUNIhiMe2YR/All%20figures%20revision%20230829.pptx

INTRODUCTION

Intercellular communication is crucial in all tissues, and especially in the tumor microenvironment, where cancer cells must instruct the surrounding stromal and immune cells to eventually form a tumor. Cells can interact with each other and with the extracellular medium through soluble secreted factors, but also through extracellular vesicles (EVs) and other non-vesicular extracellular nano-particles (NVEPs or ENPs). In the last years, the development of novel isolation and detection technologies of EVs have increased our knowledge on EVs/ENPs heterogeneity (Tkach et al., 2018; Willms et al., 2018), and highlighted the existence of novel subtypes of non-vesicular extracellular particles such as exomeres (Zhang et al., 2018), supermeres (Zhang et al., 2021b), and supramolecular attack particles (Balint et al., 2020). However, except for the latter which display killing activity, little is known still on the biological functions of these recently discovered particles (Zhang et al., 2019). In addition, most of the functional capacities attributed to EVs were observed with a mixture of EVs subtypes, ENPs and other components collectively considered as contaminants (soluble proteins, lipoproteins, etc.), raising the questions of the specific properties of each subtype of EV and ENP.

Viral infection brings an additional level of complexity to the vesicular secretome. Viruses depend on biological processes of the host cells to survive and to form viral particles. In particular, enveloped viruses are enclosed in a host cell-derived lipid bilayer which, for instance in the case of HIV, uses the EV formation machinery to be formed (Booth et al., 2006; Gould et al., 2003). Therefore, enveloped viruses can be considered as a subtype of EVs. In addition, infection by viruses modifies the amount and composition of the endogenous EVs, which can then also include viral components (Martin-Jaular et al., 2021; Nolte-'t Hoen et al., 2016). Endogenous retroviruses (ERVs) represent a potential source of enveloped viral particles and of modified endogenous EVs. ERVs are inserted in the genome of higher organisms, but are not necessarily part of a pathologic process, since they are normally mutated or repressed and thus cannot form infectious viral particles (Kassiotis and Stoye, 2017). However, their infectivity can be restored in physiological or pathological conditions, for instance in immunodeficient models or in mouse tumors (Ottina et al., 2018; Young et al., 2012).

In the tumor microenvironment, tumor cells promote changes in surrounding cells of the stroma and the immune system (Gajewski et al., 2013; Whiteside, 2008), in part through the action of EVs and ENPs (Han et al., 2019). However, the actual effects of EVs/ENPs released by tumor cells towards the immune system are controversial: there is evidence showing both immune

response activation resulting from tumor antigen transfer, and conversely, immunosuppressive functions (Greening et al., 2015; Robbins and Morelli, 2014; Thery et al., 2009). This discrepancy could be due to the different isolation methods and conditions used in these studies, leading to different combinations of heterogenous EVs, ENPs and associated contaminants, each bearing their specific and sometimes antagonist functions.

Tumor-derived EVs (endogenous or by bio-engineering) can carry antigens from the producing cells, either native or as peptides presented in MHC-I complexes on the EV membrane, and transfer it to dendritic cells (DCs), leading to a T cell-mediated antitumor response and tumor rejection (Chulpanova et al., 2018; Wolfers et al., 2001; Zeelenberg et al., 2008). Immature DCs surveil the peripheral tissues and have a high uptake capacity. Once they have captured antigens and sensed the microenvironment, they can eventually mature and migrate to lymph nodes, especially if they have detected damage, pathogen or inflammatory molecules. There, they can activate or tolerize T cells, depending on the sensed signals (Banchereau and Steinman, 1998). In addition to containing antigens, it has been proposed that EVs possess an adjuvant-intrinsic effect due to the presence of damage-associate molecular patterns (DAMPs), which may explain why EVs are more efficient than soluble proteins at transferring antigens to antigen-presenting cells (APCs) (Morelli et al., 2004; Robbins and Morelli, 2014). However, whether the antigen transfer capacities or the DAMPs are carried by all EV subtypes or ENPs, or only some specific types is unknown.

Here, we have tackled this question by first characterizing the heterogeneity of EVs and ENPs isolated from the murine mammary tumor cell line EO771. Surprisingly, we found a remarkable amount of enveloped virus-like particles (VLPs) in our preparations, that we identified as infectious retroviruses produced from endogenous murine leukemia virus (MLV). Viral gag proteins and/or VLPs were also observed in twelve other tumor cell lines, but not in two lung carcinoma and one immortalized fibroblastic cell lines. We established a protocol to reliably separate the VLPs from other small EVs and ENPs. We characterized the tumor particle subtypes by quantitative proteomic analysis and analyzed their respective capacity to transfer antigen and activate dendritic cells in vitro. Unexpectedly, our results unravel a limited potential of VLP-devoid small EVs for the induction of antigen-specific immune responses. By contrast, the large/small/VLP mixed EVs subtypes displayed the highest immune activation potential.

RESULTS

EO771 cells secrete heterogenous particles including EVs, ENPs and VLPs into the extracellular medium.

We chose the EO771 mouse cell line as a model of breast tumor cells that can be used for downstream analysis of antigen presentation in the syngeneic mouse C57BL/6 genetic background. To explore the heterogeneity of the EVs and particles secreted by EO771, we first performed a rough separation of large/medium EVs, small EVs and ENPs, based on classical differential centrifugation protocols (Jeppesen et al., 2019; Thery et al., 2006). Briefly, the serum-free conditioned medium depleted of dead cells and largest particles by a 2,000xg centrifugation was concentrated using 10 kDa filters, followed by sequential ultracentrifugation at 10,000x*g* (16 min), 200,000x*g* (50 min) and 200,000x*g* overnight (ON) to obtain pellets called 10k, 200k and ENPs respectively (Fig.1A). Nanoparticle tracking analysisshowed that, as expected, the 10k pellets contained more EVs larger than 200 nm in diameter than the 200k and ENPs (Fig EV1A). Of note, however, by NTA analysis, particles smaller than 50 nm could not be detected, and all pellets contained a majority of small EVs (< 200 nm in diameter).

The 10k, 200k and ENP pellets obtained from the same number of producing cells ($20x10^6$) were run on a western blot together with the lysate of the producing cells ($2x10^5$) and revealed with antibodies against transmembrane (CD9, CD63), external membrane-bound (Milk-fat globule-EGF-factor VIII, MFGE8), and cytosolic proteins (Alix, Ago2, Hsp90) classically used to characterize EVs and/or ENPs (Fig.1B). The total protein stain showed that ENPs contained the highest amount of proteins, followed by the 200k and 10k. However, looking at specific markers, the 200k was enriched in CD63, CD9 and MFGE8, also found in the 10k but not in the ENPs. By contrast, Alix was only detected in the 200k. Conversely, Ago2 was mainly detected in the ENPs, and to a lesser extent in the 200k. Finally, the full-length Hsp90 (*, Fig.1B) was found only in the cell lysate and the ENPs but not in the 10k or 200k, although a shorter band of around 70kDa (°, Fig.1B) was detected in the latter, probably corresponding to a previously described stress-induced cleaved form (Beck et al., 2009).

Cryo-electron microscopy (cryo-EM) (Fig.1C) revealed a great heterogeneity of particles in the 10k and 200k, including vesicles of various sizes and aspects, as well as smaller particles (10-30 nm in diameter) without any apparent lipid bilayer and aggregates of electrodense material. ENPs contained mainly the latter two structures. Surprisingly, some of the vesicles in the 10k and 200k contained circular structures with regular concentric strips (arrows and close-up in Fig.1C-D), a shape typical of viral capsids (Qu et al., 2018), suggesting the presence of virus-

like particles (VLPs). We quantified the size and the VLP aspect of the vesicles in the 200k (Fig.1D). VLP-shaped vesicles were concentrated in the range of 100-150 nm diameter (peak at 115-130 nm), consistent with the observed size of in vitro reconstituted murine leukemia virus (MLV) (Qu et al., 2018), but never observed in the smaller vesicles (25-60 up to 80 nm diameter).

To determine whether these particles were actually of viral origin, we performed a qualitative mass spectrometry-based proteomic analysis of the 200k. Mass spectrometry files were interrogated, to identify peptides from these proteins, against a data base containing the mouse proteome concatenated to protein sequences from all known mouse viruses (523 sequences manually extracted from Swissprot) and from 53 sequences of endogenous MLV envelope glycoproteins translated from the nucleotide sequences of proviruses annotated as previously described (Attig et al., 2017) (Fig EV1B, Table EV1). We detected several proteins of the family of murine leukemia virus (MLV), both exogenous (AKV, Duplan) and endogenous (Xmv, Intracisternal A-particle).

The western blot Fig.1B was further probed with antibodies against gag and envelope (env) proteins from MLV (R187 and 83A25 antibodies) (Fig.1B), which revealed the presence of both proteins in the 200k, and the 10k, but not in the ENPs. To determine whether this was a EO771 cell line-specific observation, we analyzed 13 additional mouse tumor cell lines of different genetic backgrounds and tissue origins, two non-tumoral fibroblast cell lines (Pfa1 and *Mus Dunni*), and primary splenocytes, for expression of gag and env in cell lysates (Fig EV1D) and/or 10k and 200k pellets (Fig.1E, Fig EV1B). The env protein was detected in all cells and their EV pellets by western blot and/or proteomic, except in the KP lung carcinoma cell, the *Mus Dunni* cell line and primary splenocytes. Gag was not expressed in the three cells that did not express env, nor in two cells that expressed env: LLC1 and Pfa1 (Fig.1E, Fig EV1D). All the other cell lines (12/17) expressed various levels of either full-length (Pr65) or matured (p30) gag especially in the 200k pellets. VLP structures were also observed by cryo-EM in 200k pellets of the tumor dendritic cell line MutuDC (Fig EV1C).

Finally, we evaluated the infectivity capacity of these viral particles by exposing permissive *Mus Dunni*-XG7 cells (where a GFP-encoding reporter provirus is mobilized upon retroviral infection) to the 200k of EO771 for 24h. The cell-conditioned medium (CCM) was then collected once per week during 2 weeks, and the last CCM was added to unmodified *Mus Dunni* (Young et al., 2012): detection of GFP-expressing cells in the CCM-exposed *Mus Dunni* cells confirmed the presence of infectious retroviral particles in the 200k of EO771 and of MutuDCs (Fig EV1E). Therefore, the VLP preparations also contained infectious retroviruses. However,

not knowing the proportions of infectious viruses and defective virus-like particles, we chose to use the term VLP as a generic name for both fully functional and defective viruses in the rest of the results section.

sEVs and VLPs can be separated through a velocity gradient.

Because the protocol of separation shown in Fig.1A resulted in a mix of EVs and VLPs in the 10k and 200k, we next tried to separate VLPs from the other EVs. We used EVs from EO771, as this cell line, among all the tested cells, released most abundantly gag and env proteins (Fig.1E). We first used asymmetric flow field-flow fractionation (AF4), which had been previously successfully implemented to separate exomeres (also called ENPs) and two types of EVs, respectively of 60-80 and 90-120 nm of diameter (Zhang et al., 2018). Using settings shown in Fig EV2A, we managed to separate from 200k pellets of EO771 small protein-rich structures (Fig EV2B, EV2D: P2) from light-scattering EVs, among which we recovered three populations of 35-80 nm (P3), 80-180 nm (P4) and 180-220 nm (P5) diameters (Fig EV2B-D). However, this method did not separate VLPs from small EVs of the same size, since both were identified by cryo-EM in the P4 and the P5 EV-containing AF4 fractions of the 200k pellets (Fig EV2D).

We then refined the ultracentrifugation protocol by adding an additional step of velocity gradient. We loaded the 10k (Fig EV3) or 200k (Fig.2) from EO771 cells on top of an iodixanol density gradient and centrifuged for a short time (1h30), adapting a protocol previously performed to separate HIV-1 virus from other EVs (Cantin et al., 2008; Liao et al., 2019; Martin-Jaular et al., 2021). After measuring their density (Fig.2A), we washed eight fractions of 2 ml each (1 to 8, top-to-bottom) by ultracentrifugation, resuspended them in PBS and processed for NTA measurements (Fig.2B) and western blot analysis (Fig.2C-D). Two peaks of particles were observed from the 200k: in fractions 2-3 and in fractions 56 (Fig.2B), while from the 10k, a single peak of particles was observed in the denser part, fractions 5-6 (Fig EV3A). The total protein stain of the 200k fractions showed distinct patterns of proteins in fractions 1 to 3 and 5 to 8 (Fig.2C, Fig EV3B). Remarkably, 3 prominent bands were detected in the denser fractions (5-8) but absent in the low-density fractions (1-3). We then probed the western blot with an antibody against gag of MLV (Fig.2D, Fig EV3B), revealing several bands in fractions 5 to 8, 2 of which likely corresponded to the prominent proteins (around 65kDa and 30kDa, * and ° in Fig.2C). The env MLV protein was also enriched in fractions 5-7, displaying different size variants, but it was also found in fractions 2-3 (Fig.2D, Fig EV3B). The EV markers were distributed along the 8 fractions with different abundances depending on the

marker (Fig.2D). While CD9, MFGE8 and Alix were equally present in fractions 1-3 and 5-8, CD63 and Ago2 were mostly in fractions 1-3, whereas MHC-I and the short band recognized by anti-Hsp90 (° in Fig.2E, Hsp90 panel) were most prominently detected in fractions 5-7. These results show that fractions 1 to 3 from the velocity gradient-based separation of 200k contained mainly endogenous and virus-modified sEVs, while fractions 5 to 8 contained VLPs. Fraction 4 consisted in a mixture of both. ENPs were not present in any of the fractions, probably because they were lost during the washing step performed for 50 min (rather than ON, as necessary to isolate ENPs). By contrast, the velocity gradient was not effective to separate the EVs from the VLPs in the 10k pellets, since all the particles were recovered in fractions 5-7 (Fig EV3A, B). Velocity gradient applied to 200k from Pfa1 cells showed absence of the prominent bands and of gag-labeled proteins in fractions 5-8, confirming that these cells do not release VLPs (Fig EV3C).

Thus, using a pipeline of combined protocols ((Fig.2F), we separated 3 different types of particles or vesicles: sEVs (200k velocity gradient fractions 1-3), VLPs (200k velocity gradient fractions 5-7), and ENPs (200,000xg ON pellet of the supernatant of 200,000xg 50 min, Fig.1A, Fig.2F). Additionally, we isolated two different mixtures of EVs and/or ENPs: the 10k pellet (10k) containing large/medium and small EVs plus VLPs, and a mixture of all the remaining particles pelleted by ultracentrifugation at 200,000x*g* ON of the supernatant of the 10,000x*g* centrifugation (Fig.2F). This new sample, called “Mix”, was included in the following experiments, as representative of an heterogenous mixture of particles physiologically secreted by tumor cells. We systematically recovered these 5 sample types (10k, sEVs, VLPs, ENPs, Mix) from each batch of EO771-conditioned medium, in several independent experiments. We quantified the number of particles by nanoparticle tracking analysis (NTA) and the amount of proteins recovered in each sample (Fig. EV3D, left). The Mix fraction was the most enriched in particles, while ENPs were the least enriched. By contrast, the amount of proteins was the highest in the ENPs and in the Mix. Analyzed by NTA (Fig. EV3D, right), the 10k had a significantly larger median size than sEVs and ENPs, but not significantly different from that of VLPs. The zetapotential of ENPs was significantly less negative than that of all EVs types (Fig. EV3E). Finally, only 10k and VLP preparations, but neither sEVs, nor ENPs or Mix, induced exposure of env protein on the surface of target *M. Dunni* cells after 24h of culture (Fig EV3F), suggesting that only VLPs and 10k contained infectious retroviral particles, or at least enough env to transfer it to target cells.

Quantitative proteomic analysis of the different particle subtypes

We next performed a quantitative proteomic analysis by label-free mass spectrometry on 10k, sEVs, VLPs, ENPs and Mix samples from EO771, adjusted to the same amount of proteins. Proteins were identified combining the databases of mouse and murine virus proteins as in Fig.1F. 6127 proteins in total, including 53 viral proteins, were identified by at least 3 peptides among 5 replicates in at least one type of sample (Table EV2: VennDiagram tab). Venn diagram analysis showed that most of the identified proteins (3800 total, including 35 viral proteins) were shared between all groups (Fig.3A, with Mix sample excluded from the Venn Diagram analysis for better visualization of the single fraction-specific components). Nevertheless, 303 proteins (including 4 viral) were found only in the 10k, 130 (including 1 viral) in the sEVs, 63 in the VLPs and 231 in the ENPs (Table EV2: Venn Diagram tab). Principal Component analysis (PCA) of the label-free quantification (LFQ) results (Table EV2: LFQ), showed clustering of the 5 replicates of each fraction (Fig.3B, and heatmap of protein abundance: Fig EV4A), confirming the reproducibility of our protocol. ENPs and the Mix were tightly close, indicating the prevalence of ENPs in the latter. Both were far from the membrane-containing 10k, EVs and VLPs, although to a lesser extent for the Mix, in agreement with the heterogeneous composition of this fraction which contains sEVs, VLPs and ENPs. Because of this mixed composition, the Mix was excluded from further analyses, since we aimed at identifying specific protein signatures of EV subtypes.

A Gene Ontology (GO)-term enrichment analysis was performed, first on the top-100 most abundant proteins of each group (i.e. including the shared abundant proteins) (Fig EV4B). The most significantly enriched "cellular component" GO-terms found in all samples were focal adhesion and cell-substrate junction, suggesting that areas of cell interaction with each other and with their substrate were major sources of EVs/ENPs. Other enriched GO-terms included ribosome- and nucleus-related terms, which were especially significantly enriched in sEVs and in ENPs, while terms corresponding to lumen of various internal compartments (including ficolin-1-containing compartments) were more enriched in 10K and VLPs.

We next used the state-specific protein analysis (SSPA) feature of the myProMS software (as described in Materials and Methods) to identify proteins specific to or significantly enriched in one or a group of samples (Table EV2: tab "SSPA"). GO-term enrichment analysis on the top-100 most enriched specific proteins of the 10k highlighted membranes of mitochondria, ER and secretory granules.The top-100 proteins of ENPs were enriched in GO-terms for lumen of secretory granules and lysosomes, as well as membrane of secretory and coated vesicles.sEVs top-100 proteins were enriched in nuclear components as well as both lumen and membrane components of organelles. Given the low number of specific proteins in VLPs (see Fig.3A, 3D),

only 3 significantly enriched GO-terms were identified: trans-Golgi network, and two complexes involved in regulation of transcription and histone modification (the STAGA and the SAGA complexes) (Fig.3C). Abundance of the 15 most specifically enriched proteins of each sample type (only 10 for VLPs) is shown in Fig.3D.

Finally, when we focused the analysis on the identified viral proteins (Table EV2), the majority of peptides matched with MLV proteins as identified by a few proteo-specific peptides: AKV, Duplan, but also endogenous MLV (MLV-chr5). Other viruses identified by more than one specific peptide included intracisternal a-particle, and, in lower amounts, Cas-Br-E MLV, Xmv41, lymphocytic choriomeningitis virus, murid herpes virus, mengo encephalomyocardiatis virus and murine coronavirus. The SSPA (Table EV2, Fig.3E) showed that gag-pol and pol proteins were generally enriched in both the 10k and VLPs as compared to sEVs and ENPs. The envelope proteins, by contrast, were variably distributed in all fractions. These distributions, therefore, confirmed the western blot analyses (Fig.1B, 2D, Fig EV3B). A few other viral proteins were detected, although at low levels, in sEVs and ENPs: the RNA polymerase L of the sendai and the lymphocytic choriomeningitis virus, or the replicase of coronavirus, suggesting that elements of other viruses can end up in sEVs.

Tumor derived EVs and particles induce distinct phenotypic changes in DC

Given the different protein composition of each type of particles, we hypothesized that they may induce different effects on target cells. Due to our primary interest for the role of tumor-derived EVs in establishment of antigen-specific immune responses, we chose canonical antigen presenting cells, dendritic cells (DCs), as targets of tumor-derived EVs for the subsequent functional studies. The same amount of proteins (10 or 20 μg/ml final, Fig.4B, or a dose response of 0.5 to $4x10^9$ particles corresponding to 2 to 2000 μg/ml final, Fig.4C) of each of the particle fractions produced by EO771 and characterized by proteomics as in Fig.3 (10k, sEVs, VLPs, ENPs, Mix = sEVs + VLPs + ENPs), or by Western blot as in Fig.1 (10k, 200k 50 min = sEVs + VLPs) were added for 16 h to MutuDC, a model cDC1 cell line from C57BL/6 (Fuertes Marraco et al., 2012). Then, we measured MutuDC cell viability and surface expression of maturation markers by flow cytometry (Fig EV5A, Fig.4A-G), and we quantified cytokine release in the supernatant by cytokine-bead array (CBA) (Fig.4H).

Remarkably, purified sEVs induced the death of MutuDC (Fig.4B-C, flow cytometry gating strategy shown in Fig EV5A). This toxicity was not due to insufficient washing of the iodixanol from the fractions 1-3, since it was not observed with the higher density iodixanol gradient fraction VLPs, while the 200k, containing sEVs and VLPs but devoid of any iodixanol, also

induced death (Fig.4B). We observed a very limited cytotoxic effect induced by either the 10k, VLPs, or ENPsand a low death inducing ability of Mix, probably due to the dilution of sEVs by VLPs and ENPs in this sample. Diluting sEVs with VLPs at increasing ratio (Fig.4D) reduced the toxicity of sEVs, in a manner suggesting dilution of the effect, rather than inhibition of sEVs by VLPs. Finally, this cytotoxicity was not observed at all when using EVs and particles isolated from the non-tumor cell line Pfa1 (Fig.4B), whereas it was observed when using 200k pellets from B16F10 or LLC1, but not from MCA101 nor KP (Fig.4E).

To confirm these results in a more physiological context, the EO771-derived particle treatments were applied to primary DCs isolated from the spleen of a C57BL/6 mouse (Fig EV5B-D). Basal viability of isolated DCs after 16 h of culture was low (PBS condition in Fig EV5D): 20-30% for the global DC population, with a better survival of cDC2 (60% viability). Treatment by sEVs (but not by any other samples) further decreased the viability to 10% for the global population and to 20% for cDC2. The low survival rate of pDC (20%) was decreased to 10% by treatment with any vesicle-containing samples (10k, VLPs, sEVs, Mix), but not by treatment with ENPs. Finally, the death-inducing ability of sEV was not species-specific, as it was also observed on primary DCs generated from human monocytes (Fig EV5E-F).

We then asked how EV/ENP subtypes changed the maturation profile of MutuDCs (Fig.4F-G, Fig EV5A, EV5H-I). CpG and LPS were used as internal control of DCs' ability to respond to maturation-inducing signals. Treatment by the EO771 10k pellets significantly increased expression of CD40 (Fig.4F) and MHC-II and, to a lower (and not significant) extent, of CD86 and PD-L1 (Fig EV5H). Treatment by sEVs, VLPs and 200k only slightly increased expression of CD40 and MHC-II, whereas ENPs did not induce increase of any of these markers (Fig.4F, Fig EV5H). MutuDC did not overexpress any of the analyzed co-stimulatory molecules when exposed to the Pfa1 EVs or particles (Fig.4F), while they upregulated CD40 and the other markers when exposed to 10k and (to a lower extent) 200k pellets of the 4 other mouse tumor cell lines B16F10, MCA101, LLC1, KP (Fig.4G, Fig EV5I).

A panel of 17 cytokines reported to be secreted by DCs were next quantified in the conditioned medium of MutuDC. Eight of these cytokines were detected in at least one of our samples (Fig.4H). Three of them were also detected in the EVs and ENPs that had been used for treatment of MutuDC (bottom panel Fig.4H): in particular, MCP1 was abundant in ENPs and also present in the other particles, while RANTES and IL10 were detected in all types of EVs and in ENPs but at very low level. Therefore, MCP1 detected in the supernatant of all EV-treated MutuDC was thus possibly coming from the EVs rather than from the cells, and will not be discussed further. The 10k pellet was the most efficient to induce cytokine secretion by

MutuDC, which released the 7 cytokines at a higher level than control (untreated) MutuDCs: 3 for which the difference with control treatment was statistically significant (IL6, MIP1a, MIG), 2 which were not statistically different from control but still expressed at a much higher level (TNFa, MIP1b), and 2 expressed at low level (IL10, RANTES). The second most efficient treatment was sEVs, which induced statistically significant increased secretion of MIG, and non-statistically significant (but still higher than control) levels of IL6, TNFa, MIP1b, MIP1a, RANTES. However, given the high rate of cell death observed in these cultures, some of these cytokines could have been induced by detection of cell death rather than by direct signaling induced by sEVs. VLPs induced some IL6, MIP1b and MCP1, and even smaller amounts of TNFa and MIP1a. The only cytokine detected in ENP-treated DCs was MCP1, probably coming from ENPs themselves.

In conclusion, the 10k was the most inflammatory treatment, triggering the maturation of MutuDC and the secretion of several pro-inflammatory cytokines and chemokines, whereas ENPs did not have any effect on MutuDCs, VLPs induced low levels of DC maturation, and sEVs induced some maturation and cytokine secretion, but also significant cell death. Consistent with this observation, our quantitative proteomic data showed that proteins qualifying as DAMPs and PAMPs (according to a list defined as such in (Hoshino et al., 2020)) were most abundant in the 10k pellet (Fig.4I).

Membrane-containing particles 10k, sEVs and VLPs, but not ENPs can transfer protein effectively to DCs.

A proposed mode of action of EVs is to deliver their content into target cells following their uptake. We thus wanted to compare the capacities of uptake of each of the EVs and particle subtypes. We chose the fluorescent protein, mCherry as cargo of EVs/ENPs, as it is amenable to visualization and quantification by fluorescence microscopy, flow cytometry and spectroscopy. To induce its loading into EVs/ENPs, we introduced a myristoylation and a palmitoylation sequence upstream of mCherry, to generate the myr/palm-mCherry (Fig.5A) (Mathieu et al., 2021; Valenzuela and Perez, 2020). In the resulting protein, post-translational addition of the acyl chains that insert into the cytosolic side of the lipid bilayer should lead to association of the fluorescent protein with internal membranes or lipidic structures (McCabe and Berthiaume, 1999, 2001) (Fig.5A), resulting in the targeting of this membrane-bound mCherry inside the released EVs and possibly in/on ENPs.

We transfected EO771 with a myr/palm-mCherry-expressing plasmid and we sorted mCherry$^+$ cells by flow cytometry to generate a stable cell line. We checked the cellular localization of the mCherry in the cells by confocal microscopy (Fig.5B). The mCherry fluorescence was found mainly at the plasma membrane of the cells but also internally, colocalizing partially with both CD9 and CD63.

To determine the targeting of the mCherry into the particle subtypes, the same western blot from Fig.1 and Fig.2 (which contained EV/ENP samples from myr/palm-mCherry-EO771 EVs) was revealed with an antibody against mCherry (Fig.5C): bands around 30kDa, 26 and 24kDa were detected in all particles as well as in all gradient fractions, although at different ratios. mCherry was also detected in the ENPs, mainly as the lower band form. Transmission EM analysis following immuno-labeling with anti-mCherry showed staining mostly associated to vesicles in the 10K and 200K pellets, with very few gold particles outside EVs, while most of the staining was associated to non-vesicular electron-dense structures in the ENP pellets (Fig. 5D). This staining was specific since no gold particles were observed when 10K or ENP from non-mCherry-expressing cells were analysed (suppl. Fig.1A). mCherry fluorescence was measured in each sample and compared to a standard curve of recombinant mCherry to quantify the absolute amount of mCherry. Since mCherry amount was not linearly correlated with the number of detected particles (Suppl. Fig.1B), we chose for each type of sample to use the same amount of mCherry as quantified by fluorescence, rather than the same particle number or protein amount, to feed target cells and measure efficacy of uptake.

When exposed for 16h to 10 or 30 ng of EV/ENP-associated mCherry or recombinant mCherry (rec mCherry), and analysed by flow cytometry (Fig EV5A), MutuDCs were observed to incorporate fluorescence from the 10k, sEVs, VLPs and Mix similarly and in a dose dependent manner, but not from the ENPs (Fig.5E, left). Addition of a 100-fold excess of recombinant protein (2500 ng, Fig.5E, right) was required to achieve the same degree of uptake observed with 30 ng of EV-associated mCherry.

We next performed the uptake assay with primary spleen DCs, which were exposed to 30 ng of EV/ENP-associated mCherry (Fig.5F, Fig EV5B-C). In all DC subtypes, the 10k was significantly uptaken, as compared to the PBS control and to ENPs, whereas the VLPs, sEVs, and Mix showed some level of uptake, but not significantly different from the PBS control. cDC1, the DC subtype specialized in cross-presentation, were the cells displaying the highest uptake capacity, mainly of the 10k, but also (although not significantly) of other EVs and ENPs. Our results demonstrate that the mixed EV-containing 10k is successfully captured and recognized by DCs, with a better efficiency compared to ENPs or free soluble protein.

The 10k is the scaffold that leads to the highest cross-presentation

Finally, to directly address the capacity of EVs/ENPs to induce presentation of antigens by target DCs, we used OVA as a model antigen, fused to the same myr/palm sequence used with mCherry, to allow its targeting to EVs/ENPs, and a myc tag for detection (Fig.6A). In EO771 cells stably expressing the resulting protein, OVA was detected as bands of different sizes in the secreted EVs and particles, and most prominently in the 10k (Fig.6B). The amount of OVA was quantified in each sample as compared to known concentrations of recombinant OVA loaded on the same western blot, and rapported to either the number of secreting cells (Fig.6C, left), or to the number of particles (Fig.6C, right). Like for mCherry uptake, OVA concentration was used to normalize the amount of each fraction used for the cross-presentation experiments. MutuDC cells were exposed to 1 or 2 ng of OVA associated to the different carriers for 5 h, then washed and co-cultured with OT1 cells, expressing a TCR that recognizes specifically the SIINFEKL peptide of OVA presented on MHC-I H2-Kb molecules (Fig.6D). After 18h, activation of OT1 T cells was measured by flow cytometry, quantifying expression of the activation markers CD69 and CD25 (Fig.6D-E). In this assay, the most efficient (and only statistically significant) activation of T cells was observed in the presence of MutuDC exposed to 10k. MutuDC exposed to VLPs or to Mix induced a very low, but clearly above background (although not significantly different from PBS control), level of OT1 activation, while MutuDC exposed to sEVs and ENPs did not activate at all the T cells.

DISCUSSION

Tumor-derived EVs have been proposed as a source of tumor antigen and as immune regulators in the tumor microenvironment. However, the bibliography is contradictory, attributing to tumor EVs both immuno-activating and immuno-suppressive roles (Greening et al., 2015; Robbins & Morelli, 2014; Théry et al., 2009). These discrepancies could be explained by differences in the tumor cells used as source of EVs (cell type, cancer stage, culture conditions), but also by the isolation methods, which could result in various mixtures of the EVs and ENPs that a single tumor cell secretes.

In this work, we show that the ENPs and EV subtypes from a mouse mammary adenocarcinoma cell line, EO771, have distinct and even opposite effects on target DCs in vitro. Most strikingly, we evidenced a novel, and thus far ignored, subtype of small EVs: VLPs and infectious retroviral particles, which represent a major component of these mouse tumor-derived EV preparations.

The VLPs, defined by presence of the viral capsid protein gag, come from endogenous retroviruses (ERVs) with restored infectivity. In fact, ERVs are expressed in mice at low levels, but they are non-infectious (Stocking and Kozak, 2008). However, a particular ERV locus of C57BL/6 mice, *Emv2*, encoding for an endogenous ecotropic replication-defective murine leukemia virus (eMLV) carrying a single inactivating mutation in the reverse transcriptase, can by *trans*-complementation of viral proteins and eventually recombination with other endogenous MLV proviruses, become infectious and subsequently expressed at high levels (King et al., 1988). In the organism of C57BL/6 mice, the acquisition of infectious potential of this gene is stopped by the immune system in an antibody-dependent manner (Young et al., 2012), but in *in vitro*-propagated cell lines this control process does not take place. The presence of endogenous retroviral proteins (Leong et al., 1988; Shepherd et al., 2003) and of infectious eMLV (Ottina et al., 2018) has been reported in many mouse tumor cell lines. Here, we observed expression of the env and gag MLV proteins in cells and EVs of most mouse tumor cell lines used to study cancer development (Table EV3): 12/14 of both C57Bl/6 and BalbC origin, including carcinoma, melanoma, fibrosarcoma, various hematopoietic cancer cell lines, but not in two non-tumoral fibroblasts nor in primary splenocytes . However, VLP presence in EV preparations was not strictly correlated with tumorigenicity of the cells, since we did not detect gag in two lung carcinoma (LLC1 and KP), while we had, 2 decades ago, detected gag in EV isolated from a long-term non-tumoral mouse dendritic cell line (Thery et al., 2001; Thery et al., 1999). Since endogenous retroviruses are mostly silent in the human genome (Kassiotis

and Stoye, 2017), presence of VLPs may not be as prominent in human tumor-derived cell lines, except those established from retrovirus-induced cancers. However, human endogenous retrovirus (HERV)-derived RNA and DNA have been previously detected in EVs from human gliomas and medulloblastomas (Balaj et al., 2011), and there are several reports of retroviral particle production by human placenta and cancer cells (Contreras-Galindo et al., 2008; Keydar et al., 1984; Lower et al., 1993; Nelson et al., 1978), thus calling for a more systematic assessment of the presence of VLPs and infectious retroviruses in EVs released by human tumor cell lines.

We explored the effects of the different types of EVs/ENPs on target immune cells, by designing a reliable protocol to separate the VLPs and retroviruses from other small EVs, and comparing side-by-side their effect on target antigen-presenting cells (DCs). We thus unexpectedly observed that virus-free sEVs induced death of the DCs, whereas VLPs did not display this toxic activity. The mixture of sEVs and VLPs recovered by a classical ultracentrifugation protocol (200k) also displayed some death-inducing activity, although to a lower level than the purified sEVs. Interestingly, this activity was also observed in the 200k pellets from half of the tested cell lines (Table EV3), in a manner that was neither correlated with tumorigenicity, nor with presence or not of gag or env expression. The molecular determinants of this death-inducing activity are not species-specific, since murine sEVs induced death of human DCs. They remain to be identified by follow-up studies. The list of proteins specific or strongly enriched in one or the other subtype of EVs, provided by our work (Fig.3-4, Table EV2), will be a very useful source to explore for candidate proteins responsible for these EV subtype-specific activities. However, other types of molecules, such as nucleic acids or small metabolites, could also be involved in these effects.Regarding the immunogenicity, our work shows that the 10k containing a large array of different EVs (small, large, VLPs) is the most immunogenic for DCs, promoting their maturation, cytokine and chemokine secretion, cross-presentation and activation of T cells. DC activation was observed with 10k from most tumor cell lines, whether they expressed or not VLPs, while it was not observed with 10k from the non-tumoral fibroblast Pfa1 (Table EV3). This could suggest that tumor-derived EVs have some immune functions that are tumor-specific, and that DCs are able to differentiate tumor- from non-tumor EVs, however, analysis of additional non-tumoral cell-derived 10k would be required to confirm this hypothesis. Further mechanistic studies will be required to determine the nature of the activation pathways induced by 10k in DCs, although our study provides leads.The quantitative proteomic analysis of DAMPs reveals the most rich and abundant set in the 10k, suggesting that one or several of these proteins are involved in the activation of DCs.

This enrichment could be explained by the fact that the 10k includes large EVs that might contain mitochondria or mitochondria-derived vesicles (according to the GO-term enrichment analysis, Fig.3C), or that might be plasma membrane-derived apoptotic bodies (ApoBDs, 500 nm -2 μm) coming from dying cells in the culture. ApoBDs and mitochondria are rich sources of DAMPs, and ApoBD expose phagocytotic signals and, under stress condition, induce immune activation (Caruso and Poon, 2018; Krysko et al., 2012).

On the other hand, when comparing sEVs and VLPs, we observed similar capture by MutuDCs, where both induced some surface expression of maturation markers and low levels of cytokine secretion. However, despite sEVs led to a slightly higher level of cytokine secretion than VLPs, they did not induce cross-presentation of a model antigen they had been engineered to carry, while VLPs did allow some cross-presentation. Therefore, some of the literature describing immune effects of murine tumor-"exosomes" should be reconsidered, as describing effects of a combination of toxic sEVs (possibly coming from both MVBs and the plasma membrane) and antigen-carrying VLPs and retroviruses.By contrast, the ENPs did not induce any detectable effects on the immune state of the DCs, maturation or cytokine release. This is probably due to their poor efficacy of being captured by MutuDCs, as demonstrated in our uptake assay, as opposed to the capacity of 10k, sEVs and VLPs to be uptaken (Fig.5). Therefore, even though other groups have shown that ENPs or supermeres can transfer to epithelial cells functional enzymes or receptors (Zhang et al., 2019; Zhang et al., 2021b), this activity does not seem efficient or useful on MutuDCs. Similarly, we and others have shown that the ACE2 enzyme, which is also a receptor for the SARS-CoV2 virus, is present on sEVs but also as a soluble form (Cocozza et al., 2020) or in exomeres (Zhang et al., 2021a). However, even though all forms can bind the virus (Zhang et al., 2021a), the EV-associated form is much more efficient to decrease viral infectivity (Cocozza et al., 2020). Therefore, at least for a purpose of immunogenic stimulation and antigen transfer, or for decoy activities, ENPs, like soluble recombinant proteins, are not the most promising tools.

We postulate that the presence of a lipid bilayer on all EV types makes them good targets for efficient phagocytosis. There is plenty of evidence in the literature that a lipid bilayer promotes recognition and uptake, from classic technics of cells transfection through liposomes (Lasic and Papahadjopoulos, 1995) to specific studies of uptake of nanoparticles (Mosquera et al., 2018). In addition, in EVs, the lipid bilayer contains transmembrane receptors and ligands that have counterpart receptors in membranes from target cells, thus facilitating capture. Besides these

major factors, some others might be potentiating this effect. For instance, introducing negative charges on soluble OVA antigen was shown to promote its scavenger receptor-dependent uptake by DCs (Shakushiro et al., 2004). Interestingly, we observed that all the EV/ENP subtypes were negatively charged, by measure of their zetapotential. However, the ENPs were the least electronegative and most poorly uptaken. Another feature of all the highly uptaken EV subtypes is the presence of various envelope protein of MLV. This protein can be glycosylated, which makes it recognized by lectin receptors abundantly expressed by both CD8a+ DCs (cDC1) and CD8- DCs (cDC2). In addition, the lectin receptors could also recognize other glycosylated proteins, abundant on EVs (Williams et al., 2018).

In conclusion, our work has important consequences for translation of EVs to cancer immunotherapy: a mixed preparation of large- and small-size EVs, including VLPs, corresponding to the 10k used here, seems a more efficient source of activity than highly purified small EVs or exosomes. However, this should be tested for the different producing cell sources, and the presence of infectious murine ERV, as potential factor for immune activation, would have to be demonstrated as not inducing adverse effects in humans. Conversely, our observation of the cytotoxicity of small EVs opens a new route of immunotherapy, by blocking the immunosuppressive activity of the cytotoxic tumor sEVs.

METHODS

Cells

All cells were kept at 37°C in a humidified atmosphere with 5% CO_2. The medullary breast adenocarcinoma cell line EO771 isolated as spontaneous tumor from a C57BL/6 mouse (Homburger, 1948; Sugiura and Stock, 1952) was purchased from CH3 BioSystems and cultured in RPMI-1640-Glutamax medium (Gibco) supplemented with 10% FBS (Eurobio), 10 mM HEPES (Thermo Fisher Scientific), 50 μM β-mercaptoethanol (Gibco) and 100 U/ml penicillin-streptomycin (Thermo Fisher Scientific). The Balb/c mammary carcinoma 4T1 (originating from ATCC and kindly provided by Dr S. Fiorentino) was cultured as described in (Bobrie et al., 2012) in RPMI-1640-Glutamax medium (Gibco) supplemented with 10% FBS (Eurobio), 10 mM Hepes, 100 U/mL penicillin/streptomycin and 1 mM sodium pyruvate (Thermo Fisher Scientific). The MutuDC cell line established from spleen tumors of CD11c:SV40LgT-eGFP-transgenic C57BL/6 mice was kindly provided by Dr. Hans Acha-Orbea (Fuertes Marraco et al., 2012) and cultured in IMDM (Sigma-Aldrich), supplemented with 8% FBS (Biosera), 2mM Glutamax (Gibco), 10 mM HEPES, 50 μM β-mercaptoethanol and 100 U/ml penicillin-streptomycin. The mouse spontaneously immortalized embryonic fibroblast cell line Pfa1 (Seiler et al., 2008) was kindly provided by Dr Sebastian Doll and cultured in DMEM (Thermo Fisher Scientific) supplemented with 10% FBS (Eurobio) and 100 U/ml penicillin-streptomycin. *Mus dunni* and *Mus dunni*-XG7 fibroblasts (CRL-2017) were kindly provided by Dr J.P. Stoye's lab and cultured in IMDM (Sigma-Aldrich), supplemented with 5% FBS (Eurobio), 2 mM Glutamax (Gibco), 50 μM β-mercaptoethanol and 100 U/ml penicillin-streptomycin. Various mouse cell lines available as frozen stocks in our lab were also used: B3Z was cultured in RPMI-1640-Glutamax medium (Gibco) supplemented with 10% FBS (Eurobio) and 100 U/ml penicillin-streptomycin. All other cells (TS/A, B16F10, MCA101, MB49, KP, LLC1, Raw264.7, MC38, EL4 and EG7) were cultured in DMEM (Thermo Fisher Scientific) supplemented with 10% FBS (Eurobio) and 100 U/ml penicillin-streptomycin. All cell lines were checked for mycoplasma contamination each time a batch was frozen, and found to be negative.

Mouse primary spleen DC were cultured in RPMI-1640-Glutamax medium supplemented with 10% FBS (Biosera), 1% MEM non-essential amino acids (Thermo Fisher Scientific), 1 mM sodium pyruvate, 10 mM HEPES, 50 μM β-mercaptoethanol, and 100 U/ml penicillin-streptomycin.

Human monocyte-derived DCs (MoDCs) were obtained from buffy coats from healthy human donors according to the Helsinki Declaration, with informed consent obtained from the blood donors. Briefly, peripheral blood mononuclear cells (PBMCs) were purified by density gradient centrifugation (LymphoPrep, Axis Shield) as described before (Tkach et al., 2017). CD14+ cells were enriched by magnetic sorting (CD14 Microbeads, #130-050-201 Miltenyi Biotec) following manufacturer's instructions. 20-25 million CD14+ cells were cultured in 175cm2 flasks in 30 ml of medium RPMI 1640 supplemented with 10% FCS, 10 mM Hepes, 100 IU/ml penicillin and 100 µg/ml streptomycin in the presence of IL-4 and GM-CSF (50 and 100 ng/ml, respectively; Miltenyi Biotec). After 3 days, fresh IL-4 and GM-CSF were added to the culture. Floating monocyte-derived DCs were resuspended and used 5 or 6 days after starting the culture.

Mice

OT1 mice on a Rag2 -/- C57BL/6N background (Lantz et al., 2000) were bred in the CERFE SPF animal facility (Evry, France) for Institut Curie. At 6-16 weeks age, mice were housed in the Institut Curie animal facility for at least 1 week before use. OT1 T cells were obtained by purification with EasySep^{TM} mouse naïve CD8^{+} T cell isolation kit (Stemcell) from spleen and lymph nodes of OT1 mice, according to manufacturer instructions.

PanDCs were isolated from spleen of two female C57BL/6 mice aged 14 weeks, using mouse Pan dendritic cell isolation kit according to manufacturer's instructions (Miltenyi Biotec)(Vremec and Segura, 2013).

Plasmids and generation of stable EO771 cell lines

The plasmid pmCherry-C1 from Clontech modified to add a myristoylation and palmitoylation sequence plus a linker (ATG**GGCTGCATCAAGAGCAAGCGCAAG**GACAACCTGAACGACGA CGGCGTGGACgaaccggtcgccacc) in Nterm of mCherry was kindly provided by Dr. Franck Perez (Mathieu et al., 2021; Valenzuela and Perez, 2020). myr/palm-mCherry-EO771 cells were sorted based on mCherry expression (S3^{TM} cell sorter, Bio-rad) 3 days after transfection by 5 µl of lipofectamine 2000 (Invitrogen) with 2 µg of the plasmid and regularly re-sorted to maintain expression of myr/palm-mCherry.

For myr/palm-OVA, the pTCP vector (transOMIC) was used as backbone and myristoylation and palmitoylation sequences (same as for mCherry), followed by OVA with in-frame a myc tag, the cleavage peptide P2A and puromycin resistance sequences were included in the coding frame. myr/palm-OVA-EO771 cells were obtained by selection with 4 µg/ml of puromycin, 48

hr after transduction with lentivirus from the supernatant (48 h) of HEK293FT transfected with TransIT-293 and 2 μg of the plasmids (pVSVG, pPAX2 and m/p-OVA, proportions 2:5:8). Stable cells were subsequently cultured in the presence of puromycin 2 μg/ml.

EVs and ENPs isolation by differential ultracentrifugation and density gradient

To obtain conditioned medium, EO771, Pfa1, 4T1, TS/A, B16F10, MCA101, MB49, KP, LLC1, Raw264.7, MC38 and *Mus Dunni* cells (plated 1 to 3 days before in complete medium, to reach about 80% confluency) were cultured for 24h in complete medium without serum (= serum-free medium). MutuDC were cultured for 24h in complete medium depleted from serum EV. Cell viability was measured at the end of the culture and found to be more than 85%. EV depletion from serum-containing medium was performed by overnight ultracentrifugation at 100,000x*g* in a 45Ti rotor of complete medium containing 20% FCS as described previously (Thery et al., 2006). Depleted medium was recovered by pipetting, leaving 1cm of medium above the pellet, before 0.22 μm filtration for sterilization (Liao et al., 2019). Conditioned medium was harvested and the isolation protocol was performed in sterile conditions at 4°C. The conditioned medium (90-300 ml) from 100 - 600x10^6 cells was centrifuged at 350x*g* for 10 min at 4°C. The supernatant was centrifuged at 2,000x*g* for 20 min at 4°C and the 2k pellet was discarded. The supernatant was concentrated with Millipore filters (MWCO = 10kDa, 70 ml) down to 6 ml and ultracentrifuged at 10,000x*g* for 16 min at 4°C in MLA-80 rotor (Beckman Coulter). The pellet was resuspended and washed with PBS at the same conditions (volume, speed and time), as well as for all the washes in this protocol. The obtained pellet was resuspended in PBS at 0.2 μl/10^6 cells and called 10k. The supernatant of the first 10,000x*g*, depending on the case, was divided in two: one fraction was ultracentrifuged at 200,000x*g* for 50 min at 4°C in MLA-80 rotor to obtain the 200k followed by a wash in the the same volume of PBS and the same centrifugation conditions. The 200k pellet was either resuspended at 1 μl/10^6 cells of PBS or resuspended in 1 ml of PBS to seed on top of the velocity gradient to obtain the sEVs and VLPs; the other fraction was ultracentrifuged at 200,000x*g* in MLA-80 rotor overnight at 4°C in order to obtain the Mix (washed in 6ml of PBS by overnight centrifugation at 200,000xg and resuspended at 1 μl/10^6 cells). The velocity gradient was prepared by adding 5 layers of optiprep at decreasing concentrations, bottom to top: 22%, 18%, 14%, 10% and 6% and ultracentrifuged at 187,000x*g* for 1:30h at 4°C in Sw32.1Ti rotor (Beckman Coulter). Afterwards, 8 fractions of 2 ml were collected carefully from top to bottom, washed by adding 4 ml of PBS and centrifuging at 200,000x*g* for 50 min at 4°C, and resuspended at 0.5 μl/10^6 cells of PBS. The pellets were kept separated or pooled 1-3 (sEVs)

and 5-7 (VLPs). The supernatant of the 200,000x*g* for 50 min was ultracentrifuged at 200,000x*g* in MLA-80 rotor overnight at 4°C and washed to obtain the ENPs (finally resuspended at 1 µl/10^6 cells). Samples were aliquoted and stored at -80°C.

EVs and ENPs separation by Asymetric Flow Field-Flow Fractionation (AF4)

An AF4 long channel with a frit inlet coupled to the eclipse system (Wyatt Technology, Santa Barbara, CA, USA) was driven by an isocratic pump system including a degasser and an autosampler (Shimadzu, Kyoto, Japan). Detection was performed by an ultraviolet (UV) detector at 280 nm (Shimadzu) and a multi-angle light scattering (MALS) Dawn Helios-II using a laser at 658 nm (Wyatt Technology). The channel was set up with a 350 µm spacer and a 10 kDa regenerated cellulose membrane (Wyatt Technology). PBS supplemented with 0.02% w/v NaN_3 (TCI chemicals, Tokyo, Japan) and filtered with 0.1 µm polyethersulfone filter (Sigma-Aldrich, Merck Life Science) was used as a mobile phase. All runs were performed at room temperature (20-25 °C).

A detector flow of 1 mL/min was applied in the channel and the sample was injected with an inject flow rate of 0.2 mL/min. An initial cross flow of 2 mL/min for 5 min was applied. Subsequently, the cross flow decreased exponentially from 2 mL/min to 0.1 mL/min over 50 min. The protocol was finished by cleaning the channel from all remaining components using a cross flow of 0 mL/min for 10 min. The elution inject mode was used during the entire run.

The Voyager software (Wyatt Technology) was used for data acquisition and the Astra software version 7.3.2 (Wyatt Technology) was used for data analysis. Baseline subtraction was performed. For size distribution analysis the weight density method with results fitting was applied. The sphere model was used. The refractive index for EVs (1.37) was added for correct number density estimation. Light scatter (in relative signal), diameter (in nm) and UV absorption (280nm) were plotted against time.

The AF4 eluted fractions were collected during time and pooled as indicated in Suppl. Fig.2B, and concentrated to 65 µL using Amicon Ultra-2 10K filters (Merck Life Science).

EV characterization

Western Blot

Cell lysates from $2x10^5$ cells, EVs and ENPs secreted by $20x10^6$ cells were resuspended in Laemmli sample buffer (Bio-Rad), boiled 10 min at 95°C and run in 4% - 15% Mini-Protean TGX Stain-Free gels (Bio-Rad) in non-reducing conditions (no β-mercaptoethanol nor DTT). Immuno-Blot PVDF membranes (Bio-Rad) were developed using Immobilon forte western

HRP substrate (Millipore). The antibodies used were anti-mouse: CD63 1/200 (clone R5G2, MBL, D263-3), CD9 1/1000 (clone KMC8, BD Bioscience, 553758), Alix 1/1000 (clone 3A9, Cell Signaling, 11/2012), MFGE8 1/1000 (clone 18A2-G10, MBL, D199-3), Hsp90 1/1000 (clone AC88, Enzo Lifescience, ADI-SPA-830-F), Argonaute2 1/1000 (Cell Signaling, 2897), MHC I 1/1000 (rabbit-anti-mouse MHCI, made and kindly provided by Dr H. Ploegh, Boston) (Veron et al., 2005), 14-3-3 (clone EPR6380, Abcam, ab125032). Anti p30 gag MLV 1/1000 (clone R187), env MLV 1/2000 (clone 83A25) were kindly provided by Dr Leonard Evans. Rabbit anti-OVA 1/1000 was from Rockland (200-401-033) and rabbit anti-mCherry 1/1000 from Biovision (5993).

Nanoparticle tracking analysis (NTA)

Particle concentration, size distribution and zeta potential were measured using ZetaView PMX-120 (Particle Metrix) with software version 8.04.02. Sensitivity was set at 76 and shutter at 70, 11 positions and frame rate at 30. An aliquot of 1 µl from each sample was used for the measurements and dilutions vary between 1/1000 to 1/100000 depending on the concentration of the sample.

Cryo-electron microscopy (EM)

Cryo-EM was performed on -80°C frozen samples. Lacey carbon 300 mesh grids (Ted Pella, USA) were used in all cryo-EM experiments. Blotting was carried out on the opposite side from the liquid drop and samples were plunge frozen in liquid ethane (EMGP, Leica, Germany). Cryo-EM images were acquired with a Tecnai G2 (Thermo Fisher Scientific, USA) Lab6 microscope operated at 200 kV and equipped with a 4k x 4k CMOS camera (F416, TVIPS). Image acquisition was performed under low dose conditions of 10 $e^-/Å^2$ at a magnification of 50,000 or 6,500 with a pixel size of 0.21 or 1.6 nm, respectively.

Immuno-transmission EM

Electron microscopy was performed on EV and ENP pellets from myr/palm-mCherry and myr/palm-OVA EO771 cells as control, resuspended in PBS and stored at −80 °C that had never been thawed and re-frozen. Staining with anti-mCherry antibody was performed according to the Protein A-gold method (Slot and Geuze, 2007). on EVs adsorbed for 20 min to formvar/carbon–coated copper/palladium grids followed by fixation in 2% paraformaldehyde for 20 min, saturation in PBS-glycine (5x1 min), permeabilization in PBS-BSA 1%-Saponin 0.1% or 15 min (Sigma). Immunostaining was performed by incubating with rabbit anti-

mCherry (Genetex GTX128508, 1/50) for 1 hr, 4 x 2 min washes in PBS, followed by incubation with 5 nm protein-A-gold (CMC, Utrecht, The Netherlands, 1/50) for 20 min, 3 x 5 sec + 4 x 2 min washes in PBS, and fixation for 5 min with 1% glutaraldehyde w/v in PBS (Electron Microscopy Sciences). Subsequently, after a wash on 10 droplets of distilled water, grids were transferred to droplets of 0.4% (w/v) uranyl acetate (UA) staining and 1.8% (w/v) methylcellulose embedding solution. After 10 min of incubation, grids were picked up in a wire loop. Most of the excess of the viscous embedding solution was drained away with filter paper after which the grids with sections were air-dried forming a thin layer of embedding solution. Images were acquired with a digital camera Quemesa (EMSIS GmbH, Münster, Germany) mounted on a Tecnai Spirit transmission electron microscope (FEI Company) operated at 80kV.

Protein quantification

Micro BCA^{TM} Protein Assay kit (Thermo Scientific) was used for the protein quantification. An aliquot of 1-5 μl from each sample was used for the measurements and diluted in a final volume of 150 μl.

Murine leukemia virus infectivity assay

The infectivity capacity of the MLV-containing samples was assessed as previously described (Young et al., 2012). Briefly, the 200k obtained from $10x10^6$ EO771 or MutuDC cells was added in the presence of polybrene (10 μg/ml) to $3x10^5$ *M.dunni* cells transduced with the replication defective plasmid XG7 encoding for GFP (*M.dunni-XG7*) in a 6-well plate. The cells were maintained for 14 days in culture, passaged every 2-3 days diluted 1/10-1/25, and production of the XG7 pseudotyped virus was evaluated by incubation of their supernatant with untransduced *M.dunni* cells. Briefly, $3x10^3$ *M.dunni* cells were incubated with 100 μl of supernatant in the presence of polybrene, and GFP expression was measured by flow cytometry after 3 days.

The above assay is qualitative but not quantitative. Thus, alternatively, we compared efficacy of transfer of viral env protein to target cells by flow cytometry. *Mus Dunni* cells were exposed to 0 to 40 μg/ml of the different EV subtypes in 100 μl of EV-depleted medium for 24h. Cells were then washed with PBS, trypsinized for 3 min and labeled with anti-env (83A25, 1/200) followed by anti-mouse-AF647 1/1000. Env exposure on cells was analysed by flow cytometry.

Qualitative and quantitative proteomic analyses

For the qualitative analysis (Fig.1F, Table EV1), 200k pellets from EO771, 4T1 and 200k + 10k pellets of MutuDC (10 µg, one biological replicate each) were used. For the quantitative analysis (Fig.3, Table EV2), 5 biological replicates of the 10k, sEVs, VLPs, ENPs and Mix (20 µg each) were used.

Sample Preparation: samples were resuspended in 5 µl (qualitative) or 10 µL (quantitative) (2 µg/µL) of 8 M Urea, 200 mM ammonium bicarbonate respectively. After reduction with 5 mM DTT for 30min at 57 °C and alkylation with 10 mM iodoacetamide for 30 min at room temperature in the dark, samples were diluted in 100 mM ammonium bicarbonate to reach a final concentration of 1 M urea. For the qualitative analysis, the 200k pellets were digested for 2 h at 37°C with 0.4 µg of Trypsin/Lys-C (Promega CAT#: V5071) and then overnight by adding 0.4 µg of Trypsin/Lys-C. For quantitative analyses, samples were digested overnight at 37 °C with Trypsin/Lys-C at a ratio of 1/50. Digested samples were loaded onto homemade C18 StageTips for desalting, then eluted using 40/60 MeCN/H_2O + 0.1 % formic acid and vacuum concentrated to dryness. Peptides were reconstituted in 10 µl of injection buffer in 0.3% trifluoroacetic acid (TFA) before liquid chromatography-tandem mass spectrometry (LC-MS/MS) analysis.

LC-MS/MS Analysis:

Peptides for the qualitative analysis were separated by reversed phase LC on an RSLCnano system (Ultimate 3000, Thermo Fisher Scientific) coupled online to an Orbitrap Fusion Tribrid mass spectrometer (Thermo Fisher Scientific). Peptides were trapped in a C18 column (75 µm inner diameter × 2 cm; nanoViper Acclaim PepMap 100, Thermo Fisher Scientific) with buffer A (2/98 MeCN:H2O in 0.1% formic acid) at a flow rate of 3.0 µl/min over 4 min to desalt and concentrate the samples. Separation was performed using a 40 cm × 75 µm C18 column (Reprosil C18, 1.9 µm, 120 Å, Pepsep PN: PSC-40-75-1.9-UHP-nC), regulated to a temperature of 40 °C with a linear gradient of 3% to 32% buffer B (100% MeCN in 0.1% formic acid) at a flow rate of 150 nl/min over 91 min. Full-scan MS was acquired using an Orbitrap Analyzer with the resolution set to 120,000, and ions from each full scan were higher-energy C-trap dissociation (HCD) fragmented and analysed in the linear ion trap.

For the quantitative analyses, liquid chromatography (LC) was performed as above with an RSLCnano system (Ultimate 3000, Thermo Scientific) coupled online to an Orbitrap Eclipse mass spectrometer (Thermo Fisher Scientific). Peptides were trapped onto the C18 column at a flow rate of 3.0 µL/min in buffer A for 4 min. Separation was performed on a 50 cm nanoviper column (i.d. 75 µm, C18, Acclaim PepMapTM RSLC, 2 µm, 100Å, Thermo Scientific) regulated to a temperature of 50°C with a linear gradient from 2% to 25% buffer B at a flow

rate of 300 nL/min over 91 min. MS1 data were collected in the Orbitrap (120,000 resolution; maximum injection time 60 ms; AGC 4 x 10^5). Charges states between 2 and 7 were required for MS2 analysis, and a 60 s dynamic exclusion window was used. MS2 scan were performed in the ion trap in rapid mode with HCD fragmentation (isolation window 1.2 Da; NCE 30%; maximum injection time 35 ms; AGC 10^4).

Mass Spectrometry Data analysis:

For identification, the data was searched against the *Mus musculus* (UP000000589_10090) UniProt database and a manually curated list of murine virus protein sequences using Sequest-HT through Proteome Discoverer (version 2.4). The database of murine virus proteins includes protein sequences from all known mouse endogenous and exogenous retroviruses (523 sequences manually extracted from Swissprot) and from endogenous MLV envelope glycoproteins (53 sequences), translated from the nucleotide sequences of proviruses annotated as previously described (Attig et al., 2017). Enzyme specificity was set to trypsin and a maximum of two-missed cleavage sites were allowed. Oxidized methionine, Met-loss, Met-loss-Acetyl and N-terminal acetylation were set as variable modifications. Carbamidomethylation of cysteins was set as fixed modification. Maximum allowed mass deviation was set to 10 ppm for monoisotopic precursor ions and 0.6 Da for MS/MS peaks. The resulting files were further processed using myProMS (Poullet et al., 2007) v3.9 (https://github.com/bioinfo-pf-curie/myproms). FDR calculation used Percolator (The et al., 2016) and was set to 1% at the peptide level for the whole study. Proteins were considered expressed if identified with at least 3 peptides among 5 replicates. The label free quantification was performed by peptide Extracted Ion Chromatograms (XICs), reextracted across all conditions and computed with MassChroQ version 2.2.1 (Valot et al., 2011). For protein quantification, XICs from proteotypic and non-proteotypic peptides were used by assigning to the best protein, peptides shared by multiple match groups, and missed cleavages, charge states and sources were allowed. Median and scale normalization was applied on the total signal to correct the XICs for each biological replicate (N=5) for total signal and global variance biases. Label-free quantification (LFQ) was performed following the algorithm as described (Cox et al., 2014) with the minimum number of peptide ratios set to 2 and the large ratios stabilization feature. The final LFQ intensities were used as protein abundance.

For principal component analysis (PCA), data were filtered to only allow proteins with at least 3 quantified peptide ions per sample and with all missing allowed across all samples. The LFQ values of the 3200 proteins selected were log10-transformed and the remaining (27%) missing values were imputed using the R package missMDA (Josse and Husson, 2016).

State-specific protein analysis (SSPA) is an in-house statistical assay that provides statistical ground to the potential state-specificity of a protein (typically present vs absent) based on the distribution of its missing values. To perform this test, peptides XICs are summed for each protein and the resulting value is converted into pseudo-counts by log2-transformation and background subtraction so that the lowest pseudo counts are no smaller than 1. Missing values are converted into 0. For each protein, compared states are then ordered by decreasing mean of their replicates (computed after outlier exclusion) and split into 2 sets (of states) at the largest difference between means of 2 consecutive states (largest step). The protein is declared as overexpressed in the first set and underexpressed in the second. The extent of overexpression is represented by the "best delta" which is the ratio of the largest step over the biggest mean. A statistical test relying on the general linear model with a negative binomial law is also performed to estimate the significance of the difference of means between the 2 sets. Finally, the p-values obtained for the whole dataset are corrected for multiple testing according to the Benjamini-Hochberg (FDR) method.

For heatmap representations, log10-transformed LFQ values for proteins with more than 3 peptides were used. Euclidean distances were calculated for the clustering of proteins (rows) and samples (columns). Pheatmap R package was used for representation. All proteins were used for suppl. Fig4A. The top 15 or 10 most significantly enriched proteins of each sample type (proteins with delta ≥50 ranked by adjusted p-value according to SSPA) were selected for representation in Fig.3D. The 46 quantified viral proteins were used for Fig.3E. Proteins described as DAMPs or PAMPs in (Hoshino et al., 2020) were selected for representation in Fig.4F.

GO-enrichment for Cellular Component was used in two analyses: 1) the top 100 most expressed proteins and 2) the top 100 most SSPA-specific proteins in each group of particles. Enrichr R package was used for enrichment calculations (Kuleshov et al., 2016) and ggplot2 was used for representation.

The mass spectrometry proteomics raw data are being deposited to the ProteomeXchange Consortium via the PRIDE (Perez-Riverol et al., 2022) partner repository (dataset identifier number pending).

mCherry and OVA quantification

The amount of mCherry present in each sample was quantified measuring the fluorescence (excitation 585/emission 625) of 50 µl of each sample through a spectrophotometer

(SpectraMax iD3), side-by-side with a standard curve of recombinant mCherry of known concentration.

The amount of OVA in each sample was calculated from the signal intensity of the ~ 40 kDa band, in the western blot revealed with anti-OVA antibody, using the curve of recombinant OVA with known concentration. Intensity of the bands was quantified using Image Lab software (Bio-rad).

Uptake, viability and activation assay

MutuDC or isolated murine panDC or human MoDCs were seeded at $1x10^5$ in round bottom 96 well-plates in 50 µl of complete IMDM depleted from serum-derived EVs by overnight ultracentrifugation at 100,000*xg*. Then, 1 or 2 µg of protein or 0.5 to $4x10^9$ particles corresponding to 0.2 to 200 µg of proteins, or mixtures of $4x10^9$ total particles of sEVs and VLPs in ratios ranging from 1/0 to 1/7 (for the phenotypic change assays), or 10 or 30 ng of mCherry (for the uptake assays) of the EVs and ENPs from EO771 m/p-mCherry or controls (medium alone, recombinant mCherry, LPS-EB ultrapure 10 µg/ml (Invivogen) and CpG 2 µg/ml (TriLink) were added in a final volume of 100 µl. After 16h at 37°C, cells were harvested and the supernatant was frozen for later quantification of released cytokines. For MutuDC, cells were stained with Fixable viability dye eFluor™ 780, FcR blocked and stained with fluorochrome-coupled antibodies against mouse: CD40-PerCP-eFluor710, 1/200 (46-0401-80, ThermoFisher), CD86-PE-Cy7, 1/400 (560582, BD Biosciences), PDL1-APC, 1/400 (564715, BD Biosciences) and MHC-II-eFluor 450, 1/200 (48-5320-82, ThermoFisher) or their respective isotypes controls. For panDC, cells were FcR blocked and stained with: B220-FITC, 1/200 (553087, BD Biosciences), CD11c-PerCP-Cy5.5, 1/200 (117328, BioLegend), CD86-PE-Cy7 1/400 (560582, BD Biosciences), XCR1-AF647, 1/200 (148214, BioLegend), MHC-II-APC-Cy7, 1/200 (107628, BioLegend), CD40-BV605, 1/200 (745218, BD Biosciences) and CD172a-BUV737, 1/200 (741819, BD Biosciences) or their respective isotypes controls. Cells were then stained with DAPI (source, dilution?). For human DCs, cells were stained with V525?? and fluorochrome-coupled antibodies against human: CD11c-PC7 1/200? (337216, Biolegend), CD1a-PE 1/200? (300106, Biolegend), BDCA1-PerCP eFluor710 1/200? (46-0015-42, eBioscciences), CD83-BV421 1/200? (305324, Biolegend). Cells were analyzed with a Cytoflex cytometer (Beckman). PMTs were first set following recommendation of the cytometer, and adjusted if needed to obtain signal at 0 for unstained samples and not saturated

in the positive controls. Compensation was performed with single-stained UltraComp eBeads (Thermo Fisher). Data was analyzed with FlowJo software.

Cytokine bead array

A customized set of 17 murine cytokines (IFNγ, IL2, IL5, IL4, IL6, MCP1 (CCL2), IL13, IL10, IL17a, MIP1α, TNFa, MIP1β, IL12 p70, RANTES (CCL5), MIG (CXCL9), IL1α, IL1β) reported to be secreted by DCs (Morelli et al., 2001) was selected to measure in the supernatant of the MutuDC by Cytometric Bead Array (BD CBA Flex Sets) following the manufacturer's recommendations. 15 µl of each culture supernatant was used for the assay. Samples were acquired on a BD FACS verse cytometer and analyzed with the FCAP Array software.

Cross-presentation assay

MutuDC were seeded at $1x10^4$ cells in round bottom 96 well-plates with complete EV-depleted RPMI and incubated for 5h with 1 or 2 ng of OVA in the EVs and ENPs or controls (medium alone, recombinant OVA and SIINFEKL peptide curves). After what, they were washed once with 37°C RPMI and cocultured with $5x10^4$ OT1 T cells obtained by purification with EasySep^{TM} mouse naïve $CD8^+$ T cell isolation kit (Stemcell) from spleen and lymph nodes of OT1 mice. After 16h cells were harvested and activation of the OT1 was measured by CD69 (553237, BD Pharmingen) and CD25 (551071, BD Biosciences) expression. Cells were also stained with Vα2 TCR (560624, BD Pharmingen) and CD8a (553035, BD Pharmingen) for identification. Cells were analyzed with a Cytoflex cytometer (Beckman). Data was analyzed with FlowJo software.

Data availability

Proteomic data have been deposited in PRIDE under the project accession number PXD039715. Flow Cytometry data have been deposited in FlowRepository. Imaging data have been deposited in BioIMage Archive.

ACKNOWLEDGMENTS

We thank for fruitful discussions and tools: Drs J. Helft, L. Saveanu, H. Acha-Orbea, L. Evans, J.P. Stoye, G. Boncompain, S. Doll, S. Fiorentino, L. Alaoui, M. Burbage, M. Gros, M. Jouve-San Roman, M. Rehmsmeier, L. Ringrose, and C. Basse.

This work was funded by INSERM, CNRS, Institut Curie (including NCI.NIH.PIC3i.2018), French IdEx and LabEx (ANR-10-IDEX-0001-02 PSL), the MSCA-ITN grant "TRAIN-EV" agreement No 722148, grants from fondation Chercher et Trouver, french ANR (ANR-18-CE13-0017-03; ANR-18-CE15-0008-01; ANR-18-CE16-0022-02), INCa (INCa_16083), Fondation ARC (PGA1 RF20180206962 and PGA12021020003189_3588), FRM (FDT202106013265, EQU201903007925 and DGE20121125630), Cancéropôle Île-de-France (2013-2-EML-02-ICR-1), financial support from "la Région Île-de-France" (N°EX061034) and ITMO Cancer of Aviesan and INCa on funds administered by Inserm (N°21CQ016-00) for MS analysis. We also acknowledge the following Core facilities of Institut Curie: Cell and Tissue Imaging (PICT-IBiSA), member of the French national research infrastructure France-BioImaging (ANR10-INBS-04) for fluorescence and electron microscopy, Cytometry for assistance in data acquisition, Extracellular Vesicles for assistance in EV isolation and NTA-based quantification.

CONFLICT OF INTEREST

G.K. is co-founder of EnaraBio and a member of its scientific advisory board. M.T. is currently an employee of Egle Therapeutics. Both companies are involved in search of anti-cancer therapies. The other authors have no interests to disclose.

REFERENCES

Alloatti, A., Kotsias, F., Magalhaes, J.G., and Amigorena, S. (2016). Dendritic cell maturation and cross-presentation: timing matters! Immunol Rev *272*, 97-108.

Attig, J., Young, G.R., Stoye, J.P., and Kassiotis, G. (2017). Physiological and Pathological Transcriptional Activation of Endogenous Retroelements Assessed by RNA-Sequencing of B Lymphocytes. Front Microbiol *8*, 2489.

Balaj, L., Lessard, R., Dai, L., Cho, Y.J., Pomeroy, S.L., Breakefield, X.O., and Skog, J. (2011). Tumour microvesicles contain retrotransposon elements and amplified oncogene sequences. Nat Commun *2*, 180.

Balint, S., Muller, S., Fischer, R., Kessler, B.M., Harkiolaki, M., Valitutti, S., and Dustin, M.L. (2020). Supramolecular attack particles are autonomous killing entities released from cytotoxic T cells. Science *368*, 897-901.

Banchereau, J., and Steinman, R.M. (1998). Dendritic cells and the control of immunity. Nature *392*, 245-252.

Beck, R., Verrax, J., Gonze, T., Zappone, M., Pedrosa, R.C., Taper, H., Feron, O., and Calderon, P.B. (2009). Hsp90 cleavage by an oxidative stress leads to its client proteins degradation and cancer cell death. Biochem Pharmacol *77*, 375-383.

Bobrie, A., Krumeich, S., Reyal, F., Recchi, C., Moita, L.F., Seabra, M.C., Ostrowski, M., and Thery, C. (2012). Rab27a supports exosome-dependent and -independent mechanisms that modify the tumor microenvironment and can promote tumor progression. Cancer Res *72*, 4920-4930.
Booth, A.M., Fang, Y., Fallon, J.K., Yang, J.M., Hildreth, J.E., and Gould, S.J. (2006). Exosomes and HIV Gag bud from endosome-like domains of the T cell plasma membrane. J Cell Biol *172*, 923-935.
Cantin, R., Diou, J., Belanger, D., Tremblay, A.M., and Gilbert, C. (2008). Discrimination between exosomes and HIV-1: purification of both vesicles from cell-free supernatants. J Immunol Methods *338*, 21-30.
Caruso, S., and Poon, I.K.H. (2018). Apoptotic Cell-Derived Extracellular Vesicles: More Than Just Debris. Front Immunol *9*, 1486.
Chulpanova, D.S., Kitaeva, K.V., James, V., Rizvanov, A.A., and Solovyeva, V.V. (2018). Therapeutic Prospects of Extracellular Vesicles in Cancer Treatment. Front Immunol *9*, 1534.
Cocozza, F., Nevo, N., Piovesana, E., Lahaye, X., Buchrieser, J., Schwartz, O., Manel, N., Tkach, M., Thery, C., and Martin-Jaular, L. (2020). Extracellular vesicles containing ACE2 efficiently prevent infection by SARS-CoV-2 Spike protein-containing virus. J Extracell Vesicles *10*, e12050.
Contreras-Galindo, R., Kaplan, M.H., Leissner, P., Verjat, T., Ferlenghi, I., Bagnoli, F., Giusti, F., Dosik, M.H., Hayes, D.F., Gitlin, S.D., *et al.* (2008). Human endogenous retrovirus K (HML-2) elements in the plasma of people with lymphoma and breast cancer. J Virol *82*, 9329-9336.
Cox, J., Hein, M.Y., Luber, C.A., Paron, I., Nagaraj, N., and Mann, M. (2014). Accurate proteome-wide label-free quantification by delayed normalization and maximal peptide ratio extraction, termed MaxLFQ. Mol Cell Proteomics *13*, 2513-2526.
Fuertes Marraco, S.A., Grosjean, F., Duval, A., Rosa, M., Lavanchy, C., Ashok, D., Haller, S., Otten, L.A., Steiner, Q.G., Descombes, P., *et al.* (2012). Novel murine dendritic cell lines: a powerful auxiliary tool for dendritic cell research. Front Immunol *3*, 331.
Gajewski, T.F., Schreiber, H., and Fu, Y.X. (2013). Innate and adaptive immune cells in the tumor microenvironment. Nat Immunol *14*, 1014-1022.
Gardner, A., and Ruffell, B. (2016). Dendritic Cells and Cancer Immunity. Trends Immunol *37*, 855-865.
Gould, S.J., Booth, A.M., and Hildreth, J.E. (2003). The Trojan exosome hypothesis. Proc Natl Acad Sci U S A *100*, 10592-10597.
Greening, D.W., Gopal, S.K., Xu, R., Simpson, R.J., and Chen, W. (2015). Exosomes and their roles in immune regulation and cancer. Semin Cell Dev Biol *40*, 72-81.
Han, L., Lam, E.W., and Sun, Y. (2019). Extracellular vesicles in the tumor microenvironment: old stories, but new tales. Mol Cancer *18*, 59.
Homburger, F. (1948). Studies on Hypoproteinemia: III. Lymphoid Hyperplasia and Redistribution of Nitrogen Caused in Mice by Transplanted Tumors (Sarcoma 180 and Breast Adenocarcinoma EO 771). Science *107*, 648-649.
Hoshino, A., Kim, H.S., Bojmar, L., Gyan, K.E., Cioffi, M., Hernandez, J., Zambirinis, C.P., Rodrigues, G., Molina, H., Heissel, S., *et al.* (2020). Extracellular Vesicle and Particle Biomarkers Define Multiple Human Cancers. Cell *182*, 1044-1061 e1018.
Jeppesen, D.K., Fenix, A.M., Franklin, J.L., Higginbotham, J.N., Zhang, Q., Zimmerman, L.J., Liebler, D.C., Ping, J., Liu, Q., Evans, R., *et al.* (2019). Reassessment of Exosome Composition. Cell *177*, 428-445 e418.
Josse, J., and Husson, F. (2016). missMDA: a package for handling missing values in multivariate data analysis. J Statistical Software *70*, 1-31.

Kapsenberg, M.L. (2003). Dendritic-cell control of pathogen-driven T-cell polarization. Nat Rev Immunol *3*, 984-993.
Kassiotis, G., and Stoye, J.P. (2017). Making a virtue of necessity: the pleiotropic role of human endogenous retroviruses in cancer. Philos Trans R Soc Lond B Biol Sci *372*.
Keydar, I., Ohno, T., Nayak, R., Sweet, R., Simoni, F., Weiss, F., Karby, S., Mesa-Tejada, R., and Spiegelman, S. (1984). Properties of retrovirus-like particles produced by a human breast carcinoma cell line: immunological relationship with mouse mammary tumor virus proteins. Proc Natl Acad Sci U S A *81*, 4188-4192.
King, S.R., Berson, B.J., and Risser, R. (1988). Mechanism of interaction between endogenous ecotropic murine leukemia viruses in (BALB/c X C57BL/6) hybrid cells. Virology *162*, 1-11.
Krysko, D.V., Garg, A.D., Kaczmarek, A., Krysko, O., Agostinis, P., and Vandenabeele, P. (2012). Immunogenic cell death and DAMPs in cancer therapy. Nat Rev Cancer *12*, 860-875.
Kuleshov, M.V., Jones, M.R., Rouillard, A.D., Fernandez, N.F., Duan, Q., Wang, Z., Koplev, S., Jenkins, S.L., Jagodnik, K.M., Lachmann, A., *et al.* (2016). Enrichr: a comprehensive gene set enrichment analysis web server 2016 update. Nucleic Acids Res *44*, W90-97.
Lantz, O., Grandjean, I., Matzinger, P., and Di Santo, J.P. (2000). Gamma chain required for naive CD4+ T cell survival but not for antigen proliferation. Nat Immunol *1*, 54-58.
Lasic, D.D., and Papahadjopoulos, D. (1995). Liposomes revisited. Science *267*, 1275-1276.
Leong, S.P., Muller, J., Yetter, R.A., Gorelik, E., Takami, T., and Hearing, V.J. (1988). Expression and modulation of a retrovirus-associated antigen by murine melanoma cells. Cancer Res *48*, 4954-4958.
Liao, Z., Jaular, L.M., Soueidi, E., Jouve, M., Muth, D.C., Schoyen, T.H., Seale, T., Haughey, N.J., Ostrowski, M., Thery, C., *et al.* (2019). Acetylcholinesterase is not a generic marker of extracellular vesicles. J Extracell Vesicles *8*, 1628592.
Lower, R., Boller, K., Hasenmaier, B., Korbmacher, C., Muller-Lantzsch, N., Lower, J., and Kurth, R. (1993). Identification of human endogenous retroviruses with complex mRNA expression and particle formation. Proc Natl Acad Sci U S A *90*, 4480-4484.
Martin-Jaular, L., Nevo, N., Schessner, J.P., Tkach, M., Jouve, M., Dingli, F., Loew, D., Witwer, K.W., Ostrowski, M., Borner, G.H.H., *et al.* (2021). Unbiased proteomic profiling of host cell extracellular vesicle composition and dynamics upon HIV-1 infection. EMBO J *40*, e105492.
Mathieu, M., Nevo, N., Jouve, M., Valenzuela, J.I., Maurin, M., Verweij, F.J., Palmulli, R., Lankar, D., Dingli, F., Loew, D., *et al.* (2021). Specificities of exosome versus small ectosome secretion revealed by live intracellular tracking of CD63 and CD9. Nat Commun *12*, 4389.
McCabe, J.B., and Berthiaume, L.G. (1999). Functional roles for fatty acylated amino-terminal domains in subcellular localization. Mol Biol Cell *10*, 3771-3786.
McCabe, J.B., and Berthiaume, L.G. (2001). N-terminal protein acylation confers localization to cholesterol, sphingolipid-enriched membranes but not to lipid rafts/caveolae. Mol Biol Cell *12*, 3601-3617.
Morelli, A.E., Larregina, A.T., Shufesky, W.J., Sullivan, M.L., Stolz, D.B., Papworth, G.D., Zahorchak, A.F., Logar, A.J., Wang, Z., Watkins, S.C., *et al.* (2004). Endocytosis, intracellular sorting, and processing of exosomes by dendritic cells. Blood *104*, 3257-3266.
Morelli, A.E., Zahorchak, A.F., Larregina, A.T., Colvin, B.L., Logar, A.J., Takayama, T., Falo, L.D., and Thomson, A.W. (2001). Cytokine production by mouse myeloid dendritic cells in relation to differentiation and terminal maturation induced by lipopolysaccharide or CD40 ligation. Blood *98*, 1512-1523.
Mosquera, J., Garcia, I., and Liz-Marzan, L.M. (2018). Cellular Uptake of Nanoparticles versus Small Molecules: A Matter of Size. Acc Chem Res *51*, 2305-2313.
Nelson, J., Leong, J.A., and Levy, J.A. (1978). Normal human placentas contain RNA-directed DNA polymerase activity like that in viruses. Proc Natl Acad Sci U S A *75*, 6263-6267.

Nolte-'t Hoen, E., Cremer, T., Gallo, R.C., and Margolis, L.B. (2016). Extracellular vesicles and viruses: Are they close relatives? Proc Natl Acad Sci U S A *113*, 9155-9161.
Ottina, E., Levy, P., Eksmond, U., Merkenschlager, J., Young, G.R., Roels, J., Stoye, J.P., Tuting, T., Calado, D.P., and Kassiotis, G. (2018). Restoration of Endogenous Retrovirus Infectivity Impacts Mouse Cancer Models. Cancer Immunol Res *6*, 1292-1300.
Perez-Riverol, Y., Bai, J., Bandla, C., Garcia-Seisdedos, D., Hewapathirana, S., Kamatchinathan, S., Kundu, D.J., Prakash, A., Frericks-Zipper, A., Eisenacher, M., *et al.* (2022). The PRIDE database resources in 2022: a hub for mass spectrometry-based proteomics evidences. Nucleic Acids Res *50*, D543-D552.
Poullet, P., Carpentier, S., and Barillot, E. (2007). myProMS, a web server for management and validation of mass spectrometry-based proteomic data. Proteomics *7*, 2553-2556.
Qu, K., Glass, B., Dolezal, M., Schur, F.K.M., Murciano, B., Rein, A., Rumlova, M., Ruml, T., Krausslich, H.G., and Briggs, J.A.G. (2018). Structure and architecture of immature and mature murine leukemia virus capsids. Proc Natl Acad Sci U S A *115*, E11751-E11760.
Robbins, P.D., and Morelli, A.E. (2014). Regulation of immune responses by extracellular vesicles. Nat Rev Immunol *14*, 195-208.
Seiler, A., Schneider, M., Forster, H., Roth, S., Wirth, E.K., Culmsee, C., Plesnila, N., Kremmer, E., Radmark, O., Wurst, W., *et al.* (2008). Glutathione peroxidase 4 senses and translates oxidative stress into 12/15-lipoxygenase dependent- and AIF-mediated cell death. Cell Metab *8*, 237-248.
Shakushiro, K., Yamasaki, Y., Nishikawa, M., and Takakura, Y. (2004). Efficient scavenger receptor-mediated uptake and cross-presentation of negatively charged soluble antigens by dendritic cells. Immunology *112*, 211-218.
Shepherd, A.J., Wilson, N.J., and Smith, K.T. (2003). Characterisation of endogenous retrovirus in rodent cell lines used for production of biologicals. Biologicals *31*, 251-260.
Slot, J.W., and Geuze, H.J. (2007). Cryosectioning and immunolabeling. Nat Protoc *2*, 2480-2491.
Stocking, C., and Kozak, C.A. (2008). Murine endogenous retroviruses. Cell Mol Life Sci *65*, 3383-3398.
Sugiura, K., and Stock, C.C. (1952). Studies in a tumor spectrum. I. Comparison of the action of methylbis (2-chloroethyl)amine and 3-bis(2-chloroethyl)aminomethyl-4-methoxymethyl -5-hydroxy-6-methylpyridine on the growth of a variety of mouse and rat tumors. Cancer *5*, 382-402.
The, M., MacCoss, M.J., Noble, W.S., and Kall, L. (2016). Fast and Accurate Protein False Discovery Rates on Large-Scale Proteomics Data Sets with Percolator 3.0. J Am Soc Mass Spectrom *27*, 1719-1727.
Thery, C., Amigorena, S., Raposo, G., and Clayton, A. (2006). Isolation and characterization of exosomes from cell culture supernatants and biological fluids. Curr Protoc Cell Biol *Chapter 3*, Unit 3 22.
Thery, C., Boussac, M., Veron, P., Ricciardi-Castagnoli, P., Raposo, G., Garin, J., and Amigorena, S. (2001). Proteomic analysis of dendritic cell-derived exosomes: a secreted subcellular compartment distinct from apoptotic vesicles. J Immunol *166*, 7309-7318.
Thery, C., Ostrowski, M., and Segura, E. (2009). Membrane vesicles as conveyors of immune responses. Nat Rev Immunol *9*, 581-593.
Thery, C., Regnault, A., Garin, J., Wolfers, J., Zitvogel, L., Ricciardi-Castagnoli, P., Raposo, G., and Amigorena, S. (1999). Molecular characterization of dendritic cell-derived exosomes. Selective accumulation of the heat shock protein hsc73. J Cell Biol *147*, 599-610.
Tkach, M., Kowal, J., and Thery, C. (2018). Why the need and how to approach the functional diversity of extracellular vesicles. Philos Trans R Soc Lond B Biol Sci *373*.

Tkach, M., Kowal, J., Zucchetti, A.E., Enserink, L., Jouve, M., Lankar, D., Saitakis, M., Martin-Jaular, L., and Thery, C. (2017). Qualitative differences in T-cell activation by dendritic cell-derived extracellular vesicle subtypes. EMBO J *36*, 3012-3028.
Valenzuela, J.I., and Perez, F. (2020). Localized Intercellular Transfer of Ephrin-As by Trans-endocytosis Enables Long-Term Signaling. Dev Cell *52*, 104-117 e105.
Valot, B., Langella, O., Nano, E., and Zivy, M. (2011). MassChroQ: a versatile tool for mass spectrometry quantification. Proteomics *11*, 3572-3577.
Veron, P., Segura, E., Sugano, G., Amigorena, S., and Thery, C. (2005). Accumulation of MFG-E8/lactadherin on exosomes from immature dendritic cells. Blood Cells Mol Dis *35*, 81-88.
Vremec, D., and Segura, E. (2013). The purification of large numbers of antigen presenting dendritic cells from mouse spleen. Methods Mol Biol *960*, 327-350.
Whiteside, T.L. (2008). The tumor microenvironment and its role in promoting tumor growth. Oncogene *27*, 5904-5912.
Williams, C., Royo, F., Aizpurua-Olaizola, O., Pazos, R., Boons, G.J., Reichardt, N.C., and Falcon-Perez, J.M. (2018). Glycosylation of extracellular vesicles: current knowledge, tools and clinical perspectives. J Extracell Vesicles *7*, 1442985.
Willms, E., Cabanas, C., Mager, I., Wood, M.J.A., and Vader, P. (2018). Extracellular Vesicle Heterogeneity: Subpopulations, Isolation Techniques, and Diverse Functions in Cancer Progression. Front Immunol *9*, 738.
Wolfers, J., Lozier, A., Raposo, G., Regnault, A., Thery, C., Masurier, C., Flament, C., Pouzieux, S., Faure, F., Tursz, T., *et al.* (2001). Tumor-derived exosomes are a source of shared tumor rejection antigens for CTL cross-priming. Nat Med *7*, 297-303.
Young, G.R., Eksmond, U., Salcedo, R., Alexopoulou, L., Stoye, J.P., and Kassiotis, G. (2012). Resurrection of endogenous retroviruses in antibody-deficient mice. Nature *491*, 774-778.
Zeelenberg, I.S., Ostrowski, M., Krumeich, S., Bobrie, A., Jancic, C., Boissonnas, A., Delcayre, A., Le Pecq, J.B., Combadiere, B., Amigorena, S., *et al.* (2008). Targeting tumor antigens to secreted membrane vesicles in vivo induces efficient antitumor immune responses. Cancer Res *68*, 1228-1235.
Zhang, H., Freitas, D., Kim, H.S., Fabijanic, K., Li, Z., Chen, H., Mark, M.T., Molina, H., Martin, A.B., Bojmar, L., *et al.* (2018). Identification of distinct nanoparticles and subsets of extracellular vesicles by asymmetric flow field-flow fractionation. Nat Cell Biol *20*, 332-343.
Zhang, Q., Higginbotham, J.N., Jeppesen, D.K., Yang, Y.P., Li, W., McKinley, E.T., Graves-Deal, R., Ping, J., Britain, C.M., Dorsett, K.A., *et al.* (2019). Transfer of Functional Cargo in Exomeres. Cell Rep *27*, 940-954 e946.
Zhang, Q., Jeppesen, D.K., Higginbotham, J.N., Franklin, J.L., Crowe, J.E., Jr., and Coffey, R.J. (2021a). Angiotensin-converting Enzyme 2-containing Small Extracellular Vesicles and Exomeres Bind the Severe Acute Respiratory Syndrome Coronavirus 2 Spike Protein. Gastroenterology *160*, 958-961 e953.
Zhang, Q., Jeppesen, D.K., Higginbotham, J.N., Graves-Deal, R., Trinh, V.Q., Ramirez, M.A., Sohn, Y., Neininger, A.C., Taneja, N., McKinley, E.T., *et al.* (2021b). Supermeres are functional extracellular nanoparticles replete with disease biomarkers and therapeutic targets. Nat Cell Biol *23*, 1240-1254.

FIGURE LEGENDS.

Figure 1: Characterization of the EVs and ENPs from EO771 cell line: presence of virus-like particles (VLPs). (A) Scheme of the protocol of separation of 10k, 200k and ENPs. (B) Western blot showing total proteins (left) and various protein markers as indicated (right). Lysate from $2x10^5$ EO771 cells, 10k, 200k and ENPs secreted by $20x10^6$ EO771 cells were loaded on the gel. * indicates specific Hsp90 band of the expected size. ° indicates a shorter size band resulting from endogenous cleavage. (C) Cryo-EM of EO771 10k, 200k and ENPs. Arrows indicate typical capsid-like structures inside EVs. One such structure highlighted by a white square is shown in a zoom (below, right). (D) Quantification of size and presence ("enveloped capsids") or absence (EVs) of a VLP structure in all particles of one representative sample of 200k analyzed by cryo-EM (from the image at 6,500X magnification). (E) Western blot of cell lysate (Lys) from $2x10^5$ cells, 10k and 200k secreted by $20x10^6$ of 10 tumor cell lines (EO771, TS/A, LLC1, KP, B16F10, MCA101, MB49, Raw264.7, 4T1 and MutuDC) and 2 non-tumoral fibroblast cell lines (Pfa1 and *Mus Dunni*), showing hybridization with antibodies against env (top) and gag (middle) viral proteins and total proteins (bottom). Gag is observed with different sizes, especially the full-length Pr65, and the mature cleaved p30 forms.

Figure 2: Separation of sEVs from VLPs. (A) Density of fractions of 2ml (1-8) of the velocity gradient. (B) Percentage of number of particles in each fraction over the total measured for all the gradient. n=3. (C) Protein stain-free image of a representative gel of fractions 1-8 from the gradient. * ° = prominent bands in fractions 5-7 of the same size as Pr65 and p30 gag bands in 2E. (D) Representative western blot stained with antibodies against MLV, EV and ENP markers. * ° in Hsp90 = position of full-length and short bands as observed in the 10k and 200k of Fig.1B. (E) Cryo-EM of sEVs and VLPs from EO771. (F) Summary of the different protocols used to recover 10k, 200k, sEVs, VLPs, ENPs and Mix.

Figure 3: Proteomic characterization of subtypes of particles. (A) Venn diagram of all (mouse + viral) proteins identified with at least 3 peptides among 5 replicates in at least one sample type among the 10k, sEVs, VLPs and ENPs. All proteins are listed in Table EV2, VennDiagram tab. (B) 3D view of the first 3 components of the principal component analysis (PCA) of all samples based on their protein abundance (LFQ). Samples are colored by sub-types: 10k = red; sEVs = orange, VLPs = yellow, ENPs = green, Mix = blue. (C) GO term-enrichment analysis for cellular components in the top-100 most specific proteins (from Table EV2, SSPA tab): the only 3 significant GO-terms (for VLPs) or the 15 most significant GO-terms (for 10k, sEVs and ENPs) are shown. GO-terms are ordered by adjusted.p-value. (D) Heatmap of protein abundance of the 15 most specific proteins (or the only 10 specific proteins for VLPs) of each group (from SSPA analysis, Table EV2). Clustering is shown to confirm that specific proteins are not identified due to outlier replicates. NA= not detected/absent. (E) Heatmap of protein abundance of the 46 quantified viral proteins in the different fractions. All gag-pol sequences

are primarily present in the 10k and VLPs, whereas envelope proteins (env) are more equally distributed between the fractions. NA= not detected/absent.

Figure 4: Phenotypic changes induced by the different subtypes of particles on MutuDC cells. (A) Scheme of the in vitro experiment and the parameters assessed. (B) Viability of MutuDC after 16h of exposure to 10 or 20 μg/ml of the different particles coming from EO771 (left) or Pfa1 (right), measured by flow cytometry with eFluor 780 fixable viability dye (Fig EV5A), normalized to the control non-treated condition. n=3. (C) Viability of MutuDC after 16h of exposure to 0.5, 1, 2 and $4x10^{10}$ particles/ml of the different particles coming from EO771 cells, graphed in function of their corresponding concentration of protein. n=4. (D) Viability of MutuDC cells after 16h of exposure to different ratios (1/7, 1/3, 1/1, 3/1, 7/1 and 1/0) of the mixture between sEVs and VLPs reaching 4x1010 particles/ml. (E) Viability of MutuDC after 16h of exposure to 0.5, 1, 2 and $4x10^{10}$ particles/ml of 10k and 200k coming from a panel of tumor cell lines, 3 carrying MLV gag and env in their EVs (EO771, B16F10 and MCA101), 1 carrying only env (LLC1) and 1 carrying none (KP). (F) Expression of maturation markers on viable MutuDC cells after 16 h of exposure to 10 or 20 μg/ml of the different particles coming from EO771 and Pfa1, measured by flow cytometry (Fig EV5A, GeoMean). LPS and CpG treatments were used as positive controls of maturation. n=5. (G) Expression of maturation markers on viable MutuDC cells after 16 h of exposure to 0.5, 1, 2 and $4x10^{10}$ particles/ml of the 10k and 200k coming from the same cells lines as in Fig 4E. n=3-4. (H) Quantification of cytokines secreted by DCs in the supernatant of MutuDC exposed to the subtype of particles (top) and in the particles themselves (bottom), presented as heatmap (log10 scale). "Amount 1 μg/2 μg" refers to the amount of EV/ENP used to treat MutuDC (in 100 μl final volume). n=3. Statistical analyses were performed using mixed-effects model with Dunnett's multiple comparison to the PBS, the mean of both concentrations was used for the comparisons, with different concentrations as repeated measures (B, E-G). *: $p<0.05$, **: $p< 0.01$, ***: $p< 0.001$ and ****: $p< 0.0001$. (I) Heatmap of protein abundance of proteins qualifying as DAMPs and PAMPs as quantified by LFQ in our proteomic analysis of the different types of particles (Table EV2). NA= not detected/absent.

Figure 5: Protein transfer capacity of the different subtypes of particles. (A) Scheme of the construct containing the myristoylation and palmitoylation sequences fused to mCherry, which was used to create the EO771 myr/palm-mCherry stable cells (top) and scheme of expected intracellular and intravesicular distribution of myr/palm-mCherry (bottom, created by Biorender.com). (B) Confocal microscopy of EO771-myr/palm-mCherry cells showing DAPI in blue and mCherry in red, CD9 in green and CD63 in magenta (overlay and close-ups). (C) Western blot loaded with EVs/ENPs from $20x10^6$ cells hybridized with anti-mCherry, showing its presence in the different subtypes of particles (same gels as in Fig.1B and Fig.2C,D). (D) Immunostaining with anti-mCherry (5nm gold particles) and transmission electron microscopy (TEM) analysis of saponin permeabilized 10k, 200k and ENPs from EO771 m/p-mCherry.

(E) Uptake by MutuDC, quantified by flow cytometry (expressed as % of mCherry+ cells), of 10 or 30 ng of mCherry from each subtype of particle (left, n=5), or a dose-response of recombinant mCherry (right, n=2). (F) Uptake by spleen DCs of 30 ng of mCherry from each subtype of particle. Results are presented for total CD11c+ DCs, and subtypes of DCs: cDC1, cDC2, and pDCs (defined as in Fig EV5B). One way ANOVA with Tukey's multiple comparison test was performed, n=3. *: $p<0.05$ and **: $p<0.01$.

Figure 6: Cross-presentation of OVA antigen carried by the subtypes of particles. (A) Scheme of the construct containing the myristoylation and palmitoylation sequences fused to OVA, myc tag, P2A cleavage site and puromycin resistance gene for selection, which was used to create the EO771 myr/palm-OVA stable cells. (B) Analysis of EVs/ENPs from $20x10^6$ EO771-m/p-OVA by western Blot. Four known amounts of recombinant OVA were loaded on the same gel to allow quantification of OVA. Blots were revealed with a polyclonal antibody against OVA. One representative blot out of 6. (C) Quantification of OVA in the different EVs/ENPs, was done on the western blot images as compared to the OVA dose-response curve. Graphs show ng OVA/10^6 cells (left) or ng OVA/particles (right). Friedman test with Dunn's multiple comparison was performed. n=6. (D) Scheme of the protocol of cross-presentation of EV/ENP-OVA cargo by MutuDC to OT1 T cells. (E) Dot plots of flow cytometry analysis of OTI cells (CD69 and CD25 expression), 18h after exposure to MutuDC that had been fed with OVA present in the various types of EVs/ENPs (one representative replicate). (F, G) Quantification of CD69- (F) and double CD69/CD25 (G)- expressing OT1 T cells after exposure to MutuDC that had been fed with OVA present in the various types of EVs/ENPs. Mixed- effects model was performed with Dunnett's multiple comparison to the PBS, the mean of both concentrations was used for the comparisons, with different concentrations as repeated measures, n=6. *: $p<0.05$, **: $p< 0.01$, ***: $p< 0.001$ and ****: $p< 0.0001$. (H) Cross-presentation dose-response using recombinant OVA. (I) Cross-presentation efficacy calculation using the fitting curve of the dose-response to calculate the amount of recombinant OVA needed to elicit a certain degree of activation (percentage of $CD69^+$) and dividing this value by the actual amount present in each EV/ENPs.

EXPANDED VIEW FIGURE LEGENDS

Fig EV1: Characterization and viral content evaluation of a panel of murine cells and their EVs. (A) NTA analysis of 10k, 200k and ENPs of EO771 breast tumor cells: particle quantification (left) and size distribution (right), n=4. (B) Proteomic identification of viral proteins in 200k pellets of EO771, 4T1 and MutuDC. Blue: proteins identified by specific proteotypic peptides. Green: proteins from our curated endogenous retrovirus database. (C) Western blot of cell lysate (Lys) from $2x10^5$ cells of 14 tumor cell lines (EO771, TS/A, 4T1, LLC1, KP, B16F10, MCA101, MB49, MC38, Raw264.7, MutuDC, B3Z, EL4 and EG7), 1 non-tumoral fibroblast cell line (Pfa1) and primary cell (splenocytes),

hybridized with antibodies against env and gag viral proteins and actin, as indicated. (D) Cryo-EM of 200k from MutuDC, showing presence of enveloped capsids in the former (arrows). (E) Infectivity capacity of the 200k from EO771 and MutuDC cells, shown by production of pseudotyped XG7 GFP-encoding virus from *Mus Dunni*-XG7 cells, 14 days after exposure to the EO771 or MutuDC 200k. Scheme of the protocol (left, created by Biorender.com). Pseudotyped virus in the supernatant of *Mus Dunni*-XG7 was evidenced by detection of GFP expression in parental *Mus Dunni* exposed to this supernatant (red), as compared to cells exposed to the supernatant of *Mus Dunni*-XG7 not exposed to the 200k (blue).

Fig EV2: (A) Detector-flow and cross-flow settings used for the AF4-based separation of EVs from a EO771 200k pellet. (B) UV (280 nm), Light Scattering, and particle size measured in the fractions recovered overtime (one experiment). UV signal in the absence of light scatter signal and of detected particles ≥ 35 nm (P2) corresponds to non-vesicular proteins or particles. (C) Differential weight fraction calculated from the UV (280 nm) absorption, as a function of the diameter. Two peaks of mass are observed, suggesting the presence of 2 populations of particles of around 35-80 nm and 80-180 nm, named P3 and P4. (D) cryo-EM of the total input and P1, P2, P3, P4 and P5 fractions of B, showing the presence of VLPs in both P4 and P5, together with EVs.

Fig EV3: (A) Quantification of particles in fractions recovered from an iodixanol velocity gradient top-loaded with a EO771 10k or 200k pellet from the same CM. A single peak of particles recovered in fractions 5-6 is obtained from the 10k (B) Western blot analysis of the velocity gradient fractions. Stain-free total protein (top) and hybridization with antibodies against gag and env MLV proteins or CD9 and CD63 tetraspanins (bottom). (C) Western blot analysis of the velocity gradient fractions of 200k obtained from Pfa1. Stain-free total protein stain (top) and hybridization with antibodies against gag and env MLV proteins or CD9, CD63 and Alix EV proteins (bottom). (D) Particle number (left) and protein amount (right) in each subtype of particle (10k, sEVs, VLPs, ENPs and Mix) secreted by 10^6 EO771 cells. n=13. (E) Median size (left) and zeta potential (right) of each subtype of particle. n=13. Statistical analysis. *: $p< 0.05$; **: $p<0.01$. (F) Percentage of eMLV+ *Mus Dunni* cells analysed by FACS after 24h of exposure to different amounts of proteins of 10k, sEVs, VLPs, ENPs and Mix coming from EO771 cells and staining with anti-env 83A25 antibody.

Fig EV4. Label-free quantification analysis of the proteomic results. (A) Heatmap of the protein abundance of all proteins identified in one of the 5 groups. NA= not detected/absent. (B) GO-term enrichment analysis of the top-100 most abundant proteins (according to LFQ) in the 4 groups. GO-terms with $p<0.0001$ are represented. GO-terms are ordered by adjusted.p-value.

Fig EV5: Flow cytometry gating strategy for analysis of dendritic cells' phenotype upon exposure to EVs/ENPs, and effects on primary murine and human DCs. (A) Gating strategy applied to MutuDCs to quantify viability and cell surface markers (shown in Fig.4), and mCherry uptake (shown in Fig.5). A representative example of MutuDCs exposed to 10k is shown. Blue = isotype control, red = specific antibody. (B) Gating strategy applied to spleen DCs (CD11c+) to identify DC subpopulations (cDC1 = XCR1+, cDC2 = CD172+, pDC = B220+) and viability (DAPI-). (C) Dot plot of mCherry on total viable primary DCs (CD11c+, blue arrows in EV Fig.5B) exposed to the EO771 EV/ENPs as an example of uptake. (D) Viability of isolated spleen DCs from C57BL/6 mice after 16 h of exposure to 20 μg/ml of the different particles coming from EO771tumor cells. n=3. Gating strategy follows green arrows in EV Fig.5B, i.e. gating DCs or DC subtypes before quantifying DAPI+ cells. Results are shown for total DCs (CD11c+), cDC1 (XCR1+), cDC2 (CD172a+), pDC (B220+) as indicated above each graph. n=3. (E-G) Effect of EO771-derived EVs/ENPs on human monocyte-derived DCs (MoDC). (E) Gating strategy to quantify viability and cell surface markers. (F) Viability of MoDCs exposed to $4x10^{10}$ particles/ml of EO771 EV/ENPs. (G) Percentage of activated (CD83+) MoDCs upon exposure with 20 μg/ml of EV/ENPs. (H and I) Additional maturation markers (CD86, PD-L1 and MHC-II) analyzed in parallel in the experiments of Fig.4F and G respectively.

Suppl. Fig.1: (A) Larger view and controls of the immunostaining transmission electron microscopy (TEM) with anti-mCherry perfomed on saponin permeabilized 10k, 200k and ENPs from EO771 m/p-mCherry+ and 10k and ENPs from EO771 m/p-mCherry– as control of the specificity. No gold particles are seen in the mCherry-negative samples. (B) mCherry fluorescence quantification (excitation 585/emission 625) measured with a spectrophotometer for each preparation of particle and expressed in ng, as calculated from a standard curve made with known concentration of recombinant mCherry. Results are presented as a function of the number of particles quantified by NTA in the same preparation. n=6.

Table EV1: Proteomic identification of mouse viral proteins in EV preparations from EO771 (200K pellet), 4T1 (200k pellet) and MutuDCs (10k + 200k mixed pellet) cells. Number of peptides identified in each sample (Tab: results), full list of identified proteins (Tab: all), and list of proteins identified by proteotypic peptides or as endogenous retrovirus proteins (Tab: proteotypic or endogenous, displayed in Fig. 1F) are provided.

Table EV2. Proteomic analysis results. Peptide numbers for all identified proteins, used to generate Fig.3A, are shown in "Venn Diagram" tab. Label-free quantification of each protein

is shown in “LFQ quant” tab. State-specific protein analysis (SSPA) results, to identify proteins specifically enriched in one or more sample subtypes, are shown in”SSPA” tab.

***Table EV3**. Summary of the results observed with 17 types of murine cell lines and primary cells.*

n/a: not analyzed.

Cell line	Viral components						Cytotoxicity		Activation	
	Lysate			Evs (10k+200k)						
	envMLV	gagMLV		envMLV	gagMLV					
		Pr65	p30		Pr65	p30	10k	200k	10k	200k
E0771 (mammary carcinoma, C57BL/6)	+	-	+	+++	+++	++	-	+	+++	+
TS/A (mammary adenocarcinoma, BALB/c)	+	+	-	+++	-	+	n/a	n/a	n/a	n/a
B16F10 (melanoma, C57BL/6J)	+	++	-	++	+	++	-	+	+++	+
MCA101 (sarcome, C57BL/6N)	+	+	+	++	-	+	-	-	++	+
MB49 (bladder carcinoma, C57BL/lcrfa)	+	+	+	+	-	++	n/a	n/a	n/a	n/a
RAW264.7 (tumor macrophages induced by the Abelson MLV, BALB/c)	+	-	+	+	-	+	n/a	n/a	n/a	n/a
4T1 (mammary carcinoma, BALB/c)	+	+	-	+	+	+	n/a	n/a	n/a	n/a
MutuDC (tumor dendritic cells induced by SV40, C57BL/6)	+	-	-	+	++	+	n/a	n/a	n/a	n/a
MC38 (colon adenocarcinoma, C57BL/6)	+	-	+	n/a	n/a	n/a	n/a	n/a	n/a	n/a
B3Z (T cell hybridoma, AKR/J)	+	+	+	n/a	n/a	n/a	n/a	n/a	n/a	n/a
EL4 (T cell lymphoma, C57BL/6N)	+	+	-	n/a	n/a	n/a	n/a	n/a	n/a	n/a
EG7 (T cell lymphoma, C57BL/6N)	+	+	-	n/a	n/a	n/a	n/a	n/a	n/a	n/a
LLC1 (Lewis lung carcinoma, C57BL)	+	-	-	++	-	-	-	+	+++	+
Pfa1 (embryonic fibroblast, C57BL/6)	+	-	-	+	-	-	-	-	-	-
KP (lung adenocarcinoma, C57BL/6)	-	-	-	-	-	-	-	-	+	+
Mus Dunni (fibroblast, Mus Terricolor)	-	-	-	-	-	-	n/a	n/a	n/a	n/a
Splenocytes (C57BL/6)	-	-	-	n/a	n/a	n/a	n/a	n/a	n/a	n/a
Tumor cell line										
env + gag +										
env + gag -										
env - gag -										

Figure 1

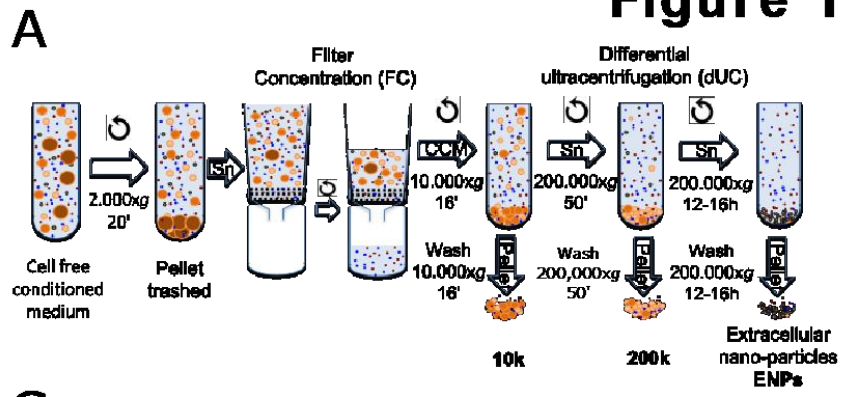

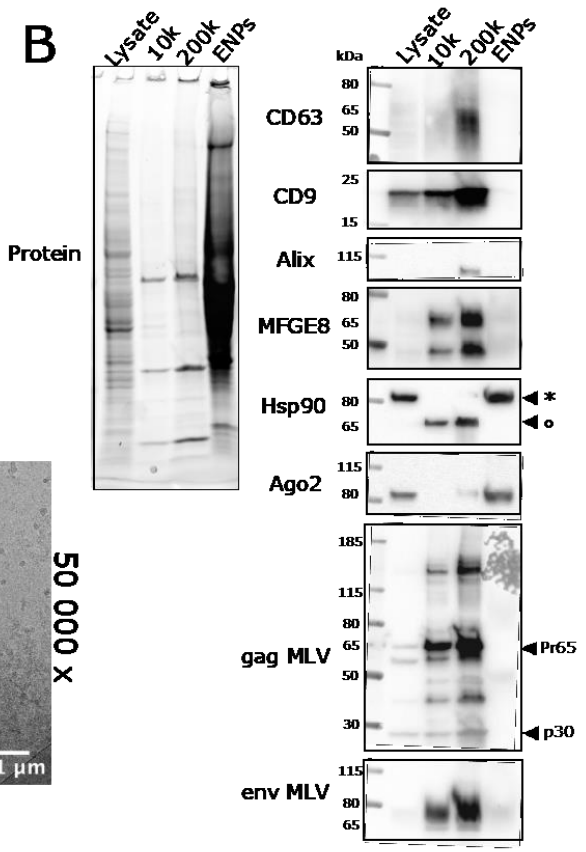

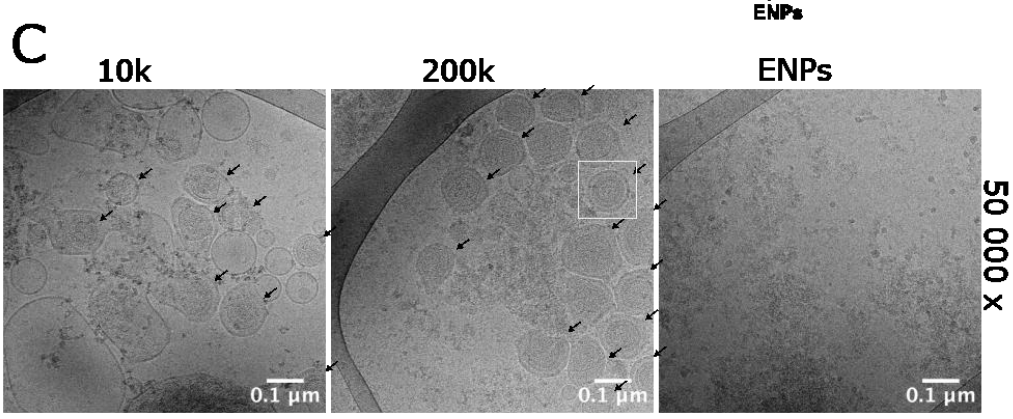

↙= envelopped capsid

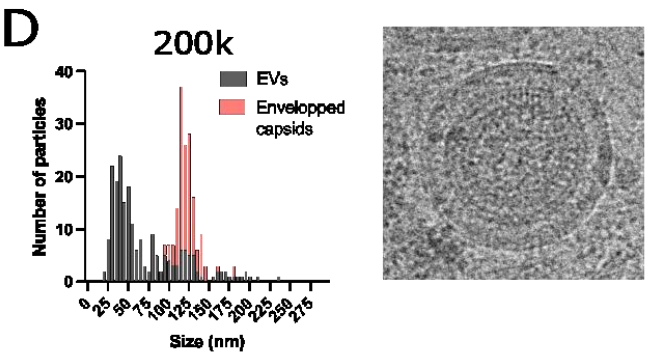

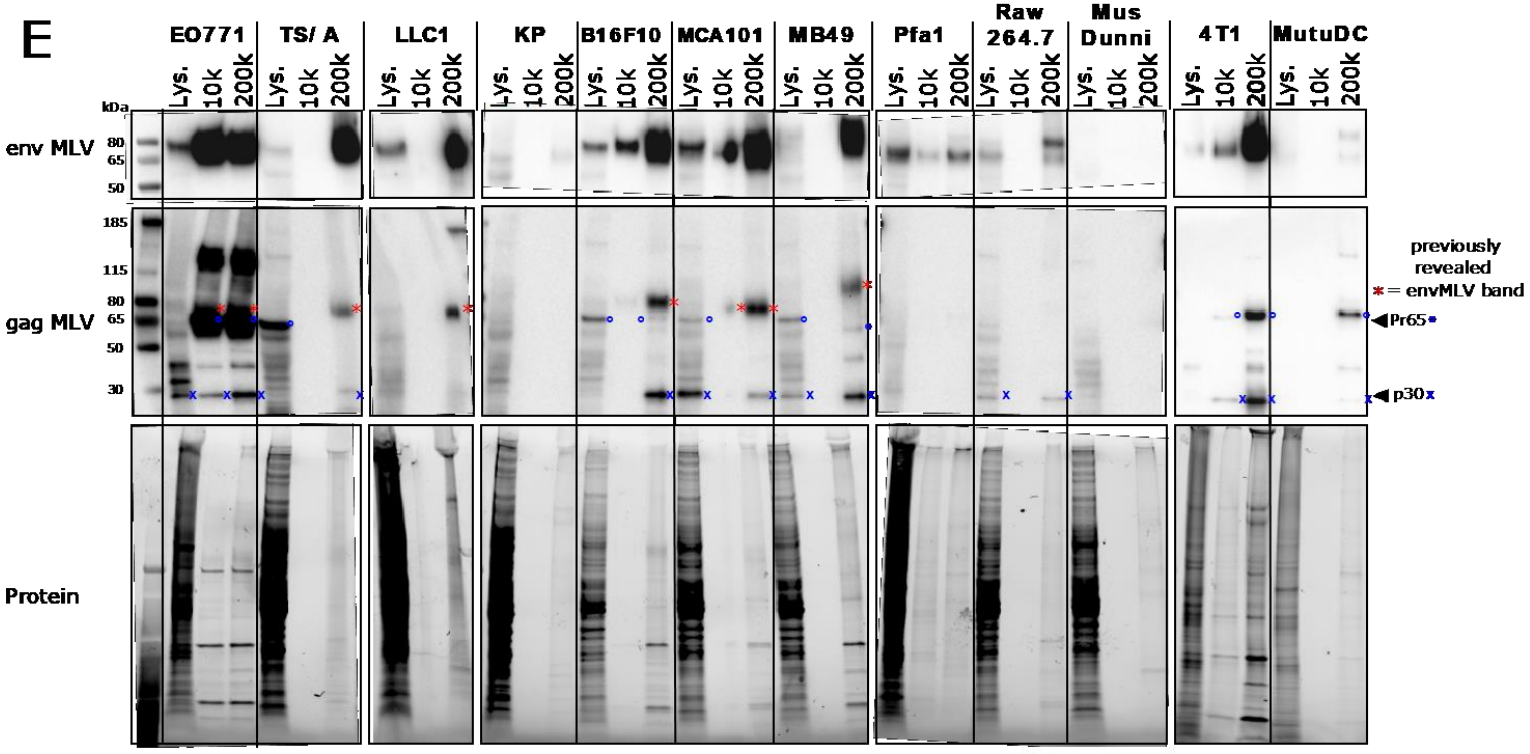

Extended view 1

A

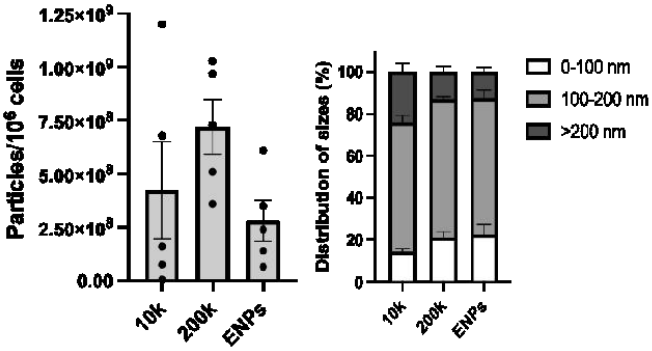

B

Proteins	Peptides			Description	Species
	E0771	4T1	Mutu DC		
pol	77	14	31	Gag-Pol polyprotein	AKV murine leukemia
gag-pol	74	8	26	Gag-pol polyprotein	Murine leukemia virus
pol	59		23	Gag-Pol polyprotein	Radiation murine leukemia
P0DOG8	42	13	25	Glyco-Gag protein	AKV murine leukemia
gag	23	8	20	Gag polyprotein	Duplan murine leukemia
env_of_MLV_Xmv45	17		18		Mus Musculus
Emv2_consensus_env	16	8			Mus Musculus
P12894	15	1		Intracisternal A-particle Pol-related polyprotein (Fragment)	Mouse intracisternal a-particle IL3
env_of_Xmv10	10		13		Mus Musculus
env_of_MLV_Xmv43			15		Mus Musculus
env_of_Pmv1			11		Mus Musculus
M45			1	Ribonucleoside-diphosphate reductase large subunit-like protein	Murid herpesvirus 1

endogenous
proteotypic

C

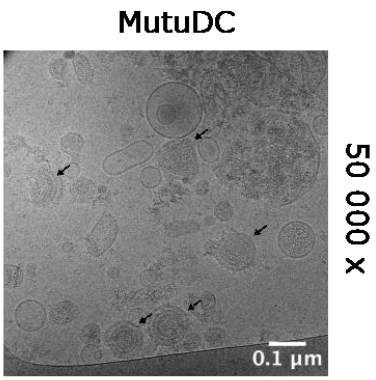

↙ = envelopped capsid

D

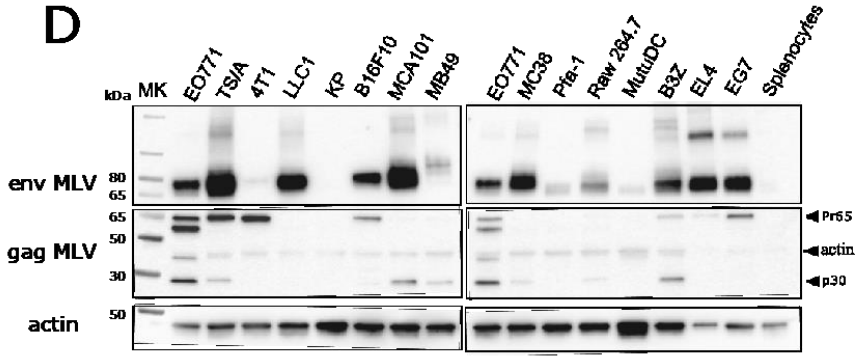

E

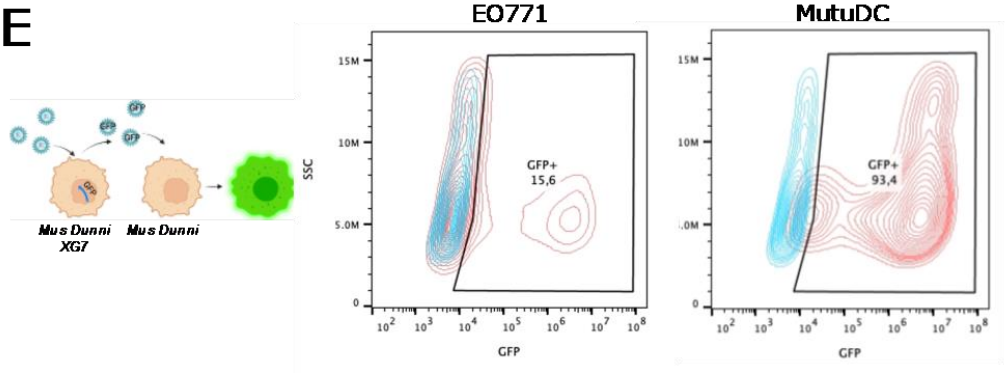

Extended view 2

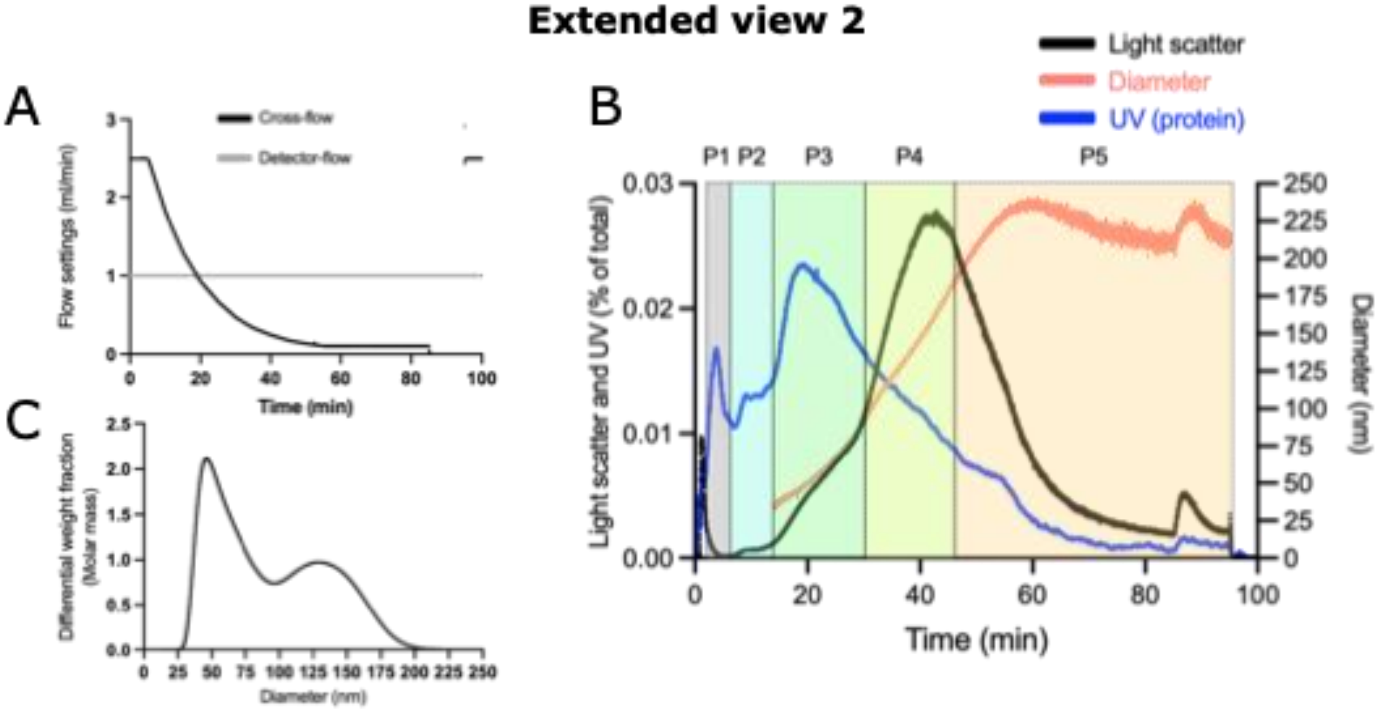

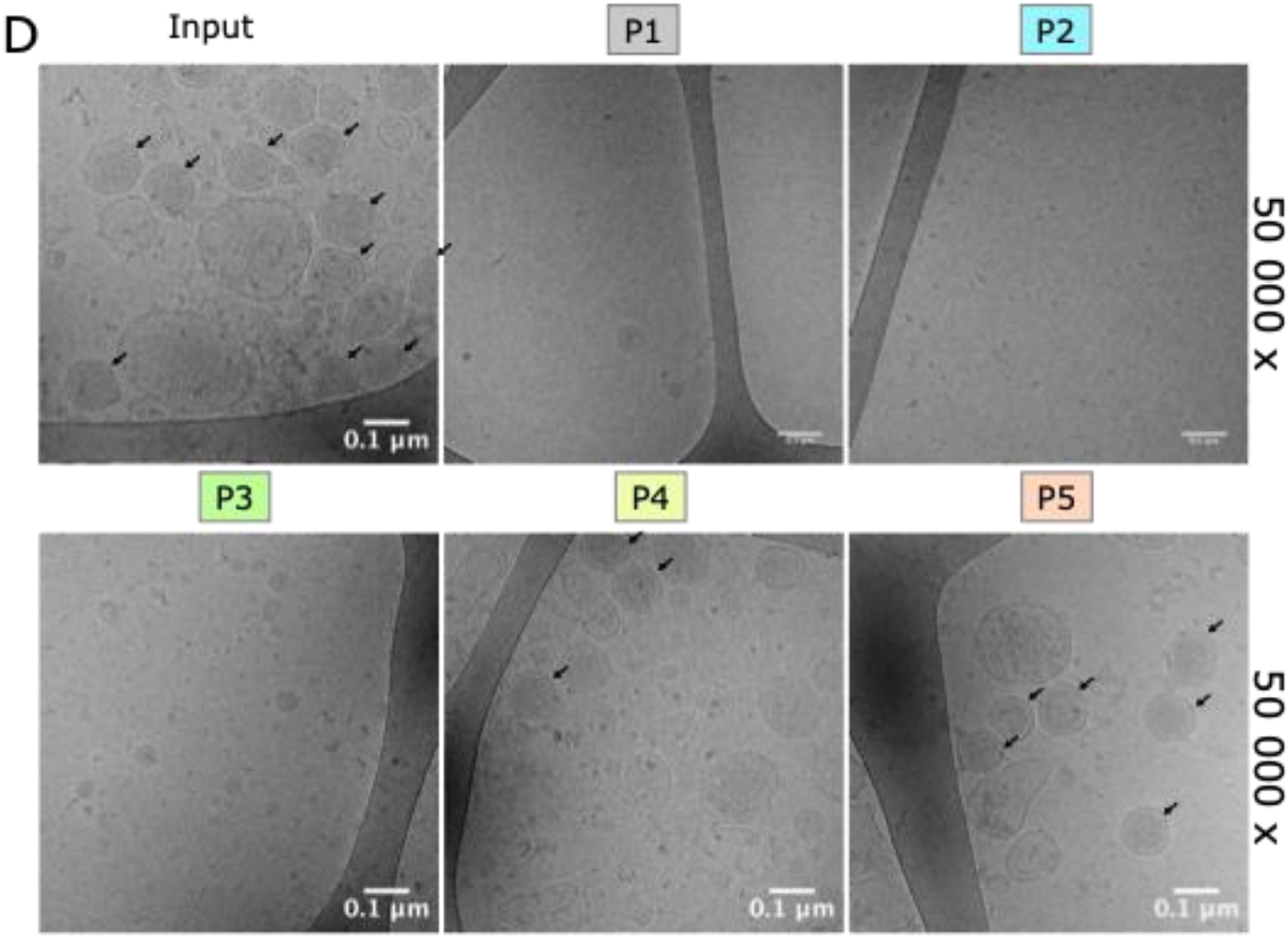

↙ = envelopped capsid

Figure 2

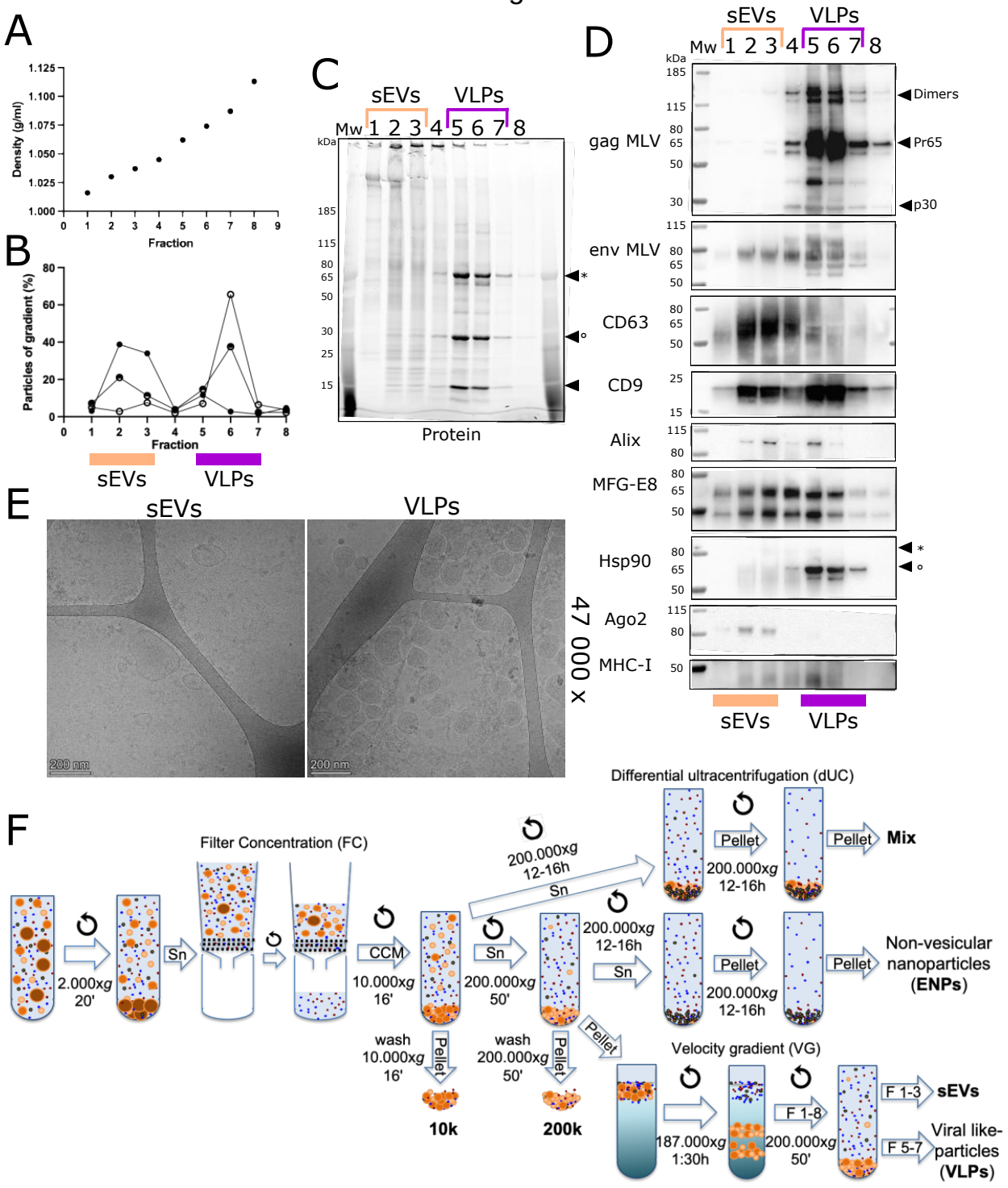
A
Density (g/ml)
Fraction
B
Particles of gradient (%)
Fraction
sEVs
VLPs
C
sEVs
VLPs
Mw 1 2 3 4 5 6 7 8
kDa
Protein
D
sEVs
VLPs
Mw 1 2 3 4 5 6 7 8
kDa
gag MLV
Dimers
Pr65
p30
env MLV
CD63
CD9
Alix
MFG-E8
Hsp90
Ago2
MHC-I
sEVs
VLPs
E
sEVs
VLPs
200 nm
47 000 x
F
Filter Concentration (FC)
2.000xg 20'
Sn
CCM 10.000xg 16'
wash 10.000xg 16'
Pellet
10k
Sn
200.000xg 50'
wash 200.000xg 50'
Pellet
200k
200.000xg 12-16h
Sn
Differential ultracentrifugation (dUC)
Pellet
200.000xg 12-16h
Pellet
Mix
Pellet
200.000xg 12-16h
Pellet
Non-vesicular nanoparticles (ENPs)
Pellet
Velocity gradient (VG)
187.000xg 1:30h
F 1-8
200.000xg 50'
F 1-3
sEVs
F 5-7
Viral like-particles (VLPs)

Extended view 3

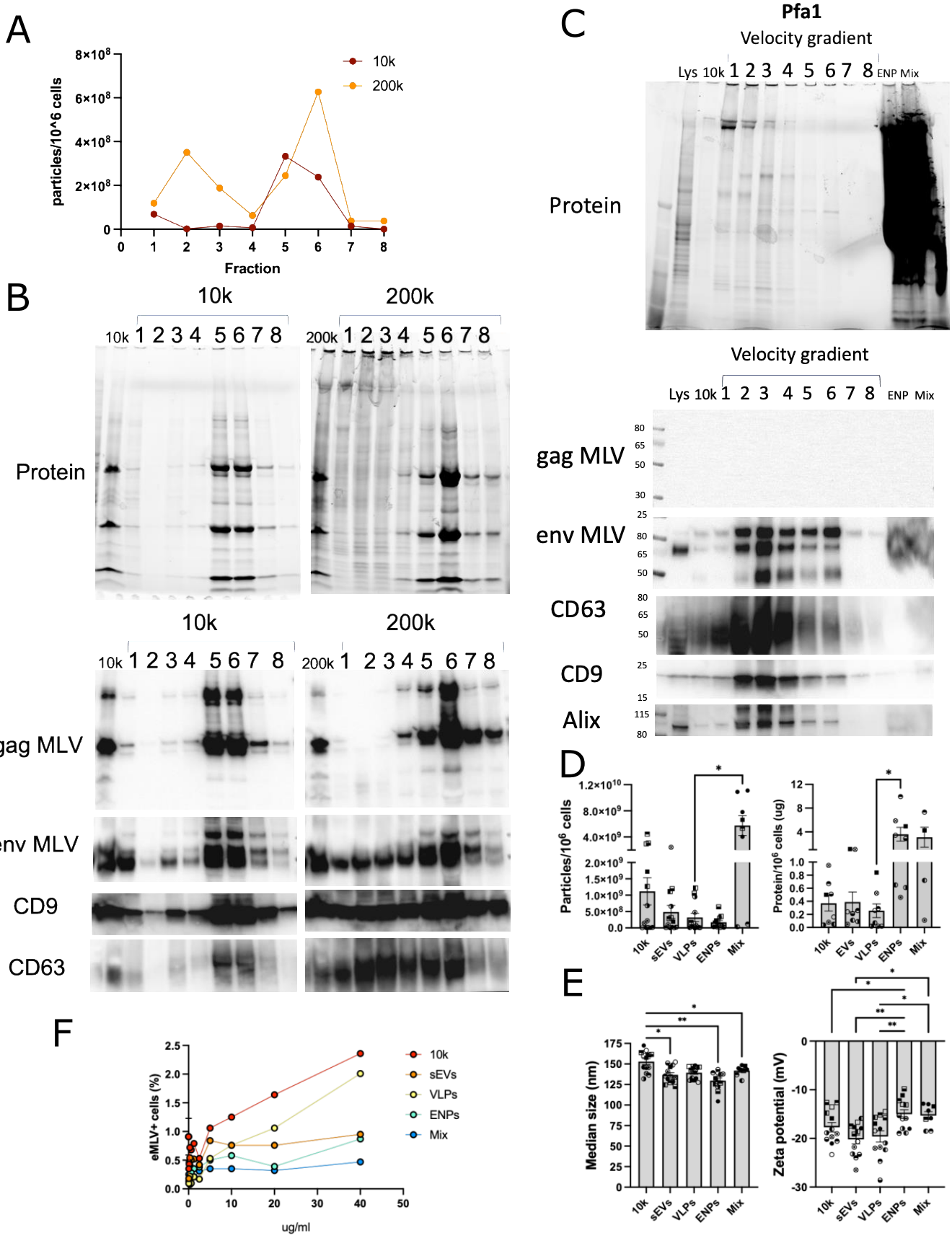

Figure 3

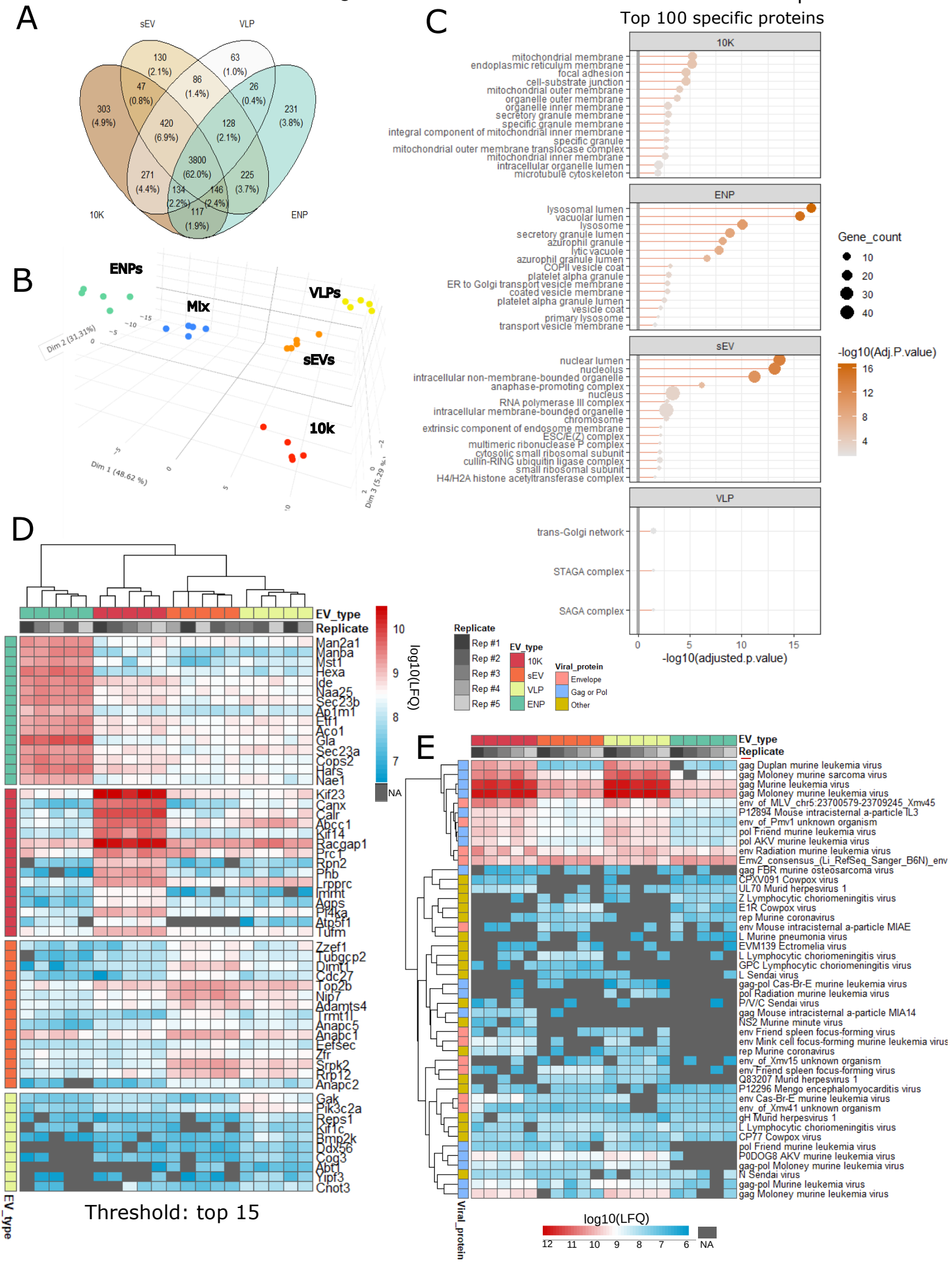
A
sEV
VLP
10K
ENP
130 (2.1%)
63 (1.0%)
47 (0.8%)
86 (1.4%)
26 (0.4%)
303 (4.9%)
420 (6.9%)
128 (2.1%)
231 (3.8%)
3800 (62.0%)
271 (4.4%)
134 (2.2%)
146 (2.4%)
225 (3.7%)
117 (1.9%)
B
ENPs
Mix
VLPs
sEVs
10k
Dim 1 (48.62 %)
Dim 2 (31.31%)
Dim 3 (5.29 %)
C
GO term: cellular component
Top 100 specific proteins
10K
mitochondrial membrane
endoplasmic reticulum membrane
focal adhesion
cell-substrate junction
mitochondrial outer membrane
organelle outer membrane
organelle inner membrane
secretory granule membrane
specific granule membrane
integral component of mitochondrial inner membrane
specific granule
mitochondrial outer membrane translocase complex
mitochondrial inner membrane
intracellular organelle lumen
microtubule cytoskeleton
ENP
lysosomal lumen
vacuolar lumen
lysosome
secretory granule lumen
azurophil granule
lytic vacuole
azurophil granule lumen
COPII vesicle coat
platelet alpha granule
ER to Golgi transport vesicle membrane
coated vesicle membrane
platelet alpha granule lumen
vesicle coat
primary lysosome
transport vesicle membrane
sEV
nuclear lumen
nucleolus
intracellular non-membrane-bounded organelle
anaphase-promoting complex
nucleus
RNA polymerase III complex
intracellular membrane-bounded organelle
chromosome
extrinsic component of endosome membrane
ESC/E(Z) complex
multimeric ribonuclease P complex
cytosolic small ribosomal subunit
cullin-RING ubiquitin ligase complex
small ribosomal subunit
H4/H2A histone acetyltransferase complex
VLP
trans-Golgi network
STAGA complex
SAGA complex
-log10(adjusted.p.value)
Gene_count
10
20
30
40
-log10(Adj.P.value)
16
12
8
4
Replicate
Rep #1
Rep #2
Rep #3
Rep #4
Rep #5
EV_type
10K
sEV
VLP
ENP
Viral_protein
Envelope
Gag or Pol
Other
D
EV_type
Replicate
Man2a1
Manba
Mst1
Hexa
Ide
Naa25
Sec23b
Ap1m1
Etf1
Aco1
Gla
Sec23a
Cops2
Hars
Nae1
Kif23
Canx
Calr
Abcc1
Kif14
Racgap1
Prc1
Rpn2
Phb
Lrpprc
Immt
Aggs
Pi4ka
Atp5f1
Tufm
Zzef1
Tubgcp2
Dimt1
Cdc27
Top2b
Nip7
Adamts4
Trmt1l
Anapc5
Anapc1
Eefsec
Zfr
Srpk2
Rrp12
Anapc2
Gak
Pik3c2a
Reps1
Kif1c
Bmp2k
Ddx56
Cog3
Abt1
Yipf3
Chot3
log10(LFQ)
10
9
8
7
NA
EV_type
Threshold: top 15
E
EV_type
Replicate
gag Duplan murine leukemia virus
gag Moloney murine sarcoma virus
gag Murine leukemia virus
gag Moloney murine leukemia virus
env_of_MLV_chr5:23700579-23709245_Xmv45
P12894 Mouse intracisternal a-particle IL3
env_of_Pmv1 unknown organism
pol Friend murine leukemia virus
pol AKV murine leukemia virus
env Radiation murine leukemia virus
Emv2_consensus_(Li_RefSeq_Sanger_B6N)_env
gag FBR murine osteosarcoma virus
CPXV091 Cowpox virus
UL70 Murid herpesvirus 1
Z Lymphocytic choriomeningitis virus
E1R Cowpox virus
rep Murine coronavirus
env Mouse intracisternal a-particle MIAE
L Murine pneumonia virus
EVM139 Ectromelia virus
L Lymphocytic choriomeningitis virus
GPC Lymphocytic choriomeningitis virus
L Sendai virus
gag-pol Cas-Br-E murine leukemia virus
pol Radiation murine leukemia virus
P/V/C Sendai virus
gag Mouse intracisternal a-particle MIA14
NS2 Murine minute virus
env Friend spleen focus-forming virus
env Mink cell focus-forming murine leukemia virus
rep Murine coronavirus
env_of_Xmv15 unknown organism
env Friend spleen focus-forming virus
Q83207 Murid herpesvirus 1
P12296 Mengo encephalomyocarditis virus
env Cas-Br-E murine leukemia virus
env_of_Xmv41 unknown organism
gH Murid herpesvirus 1
L Lymphocytic choriomeningitis virus
CP77 Cowpox virus
pol Friend murine leukemia virus
P0DOG8 AKV murine leukemia virus
gag-pol Moloney murine leukemia virus
N Sendai virus
gag-pol Murine leukemia virus
gag Moloney murine leukemia virus
Viral_protein
log10(LFQ)
12
11
10
9
8
7
6
NA

Extended view 4

A

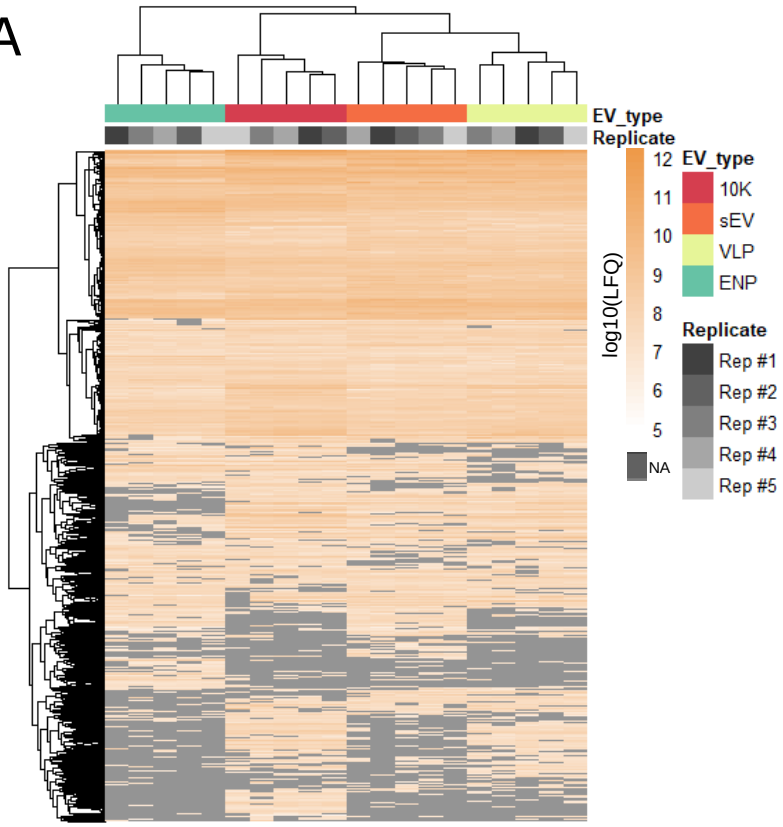

B

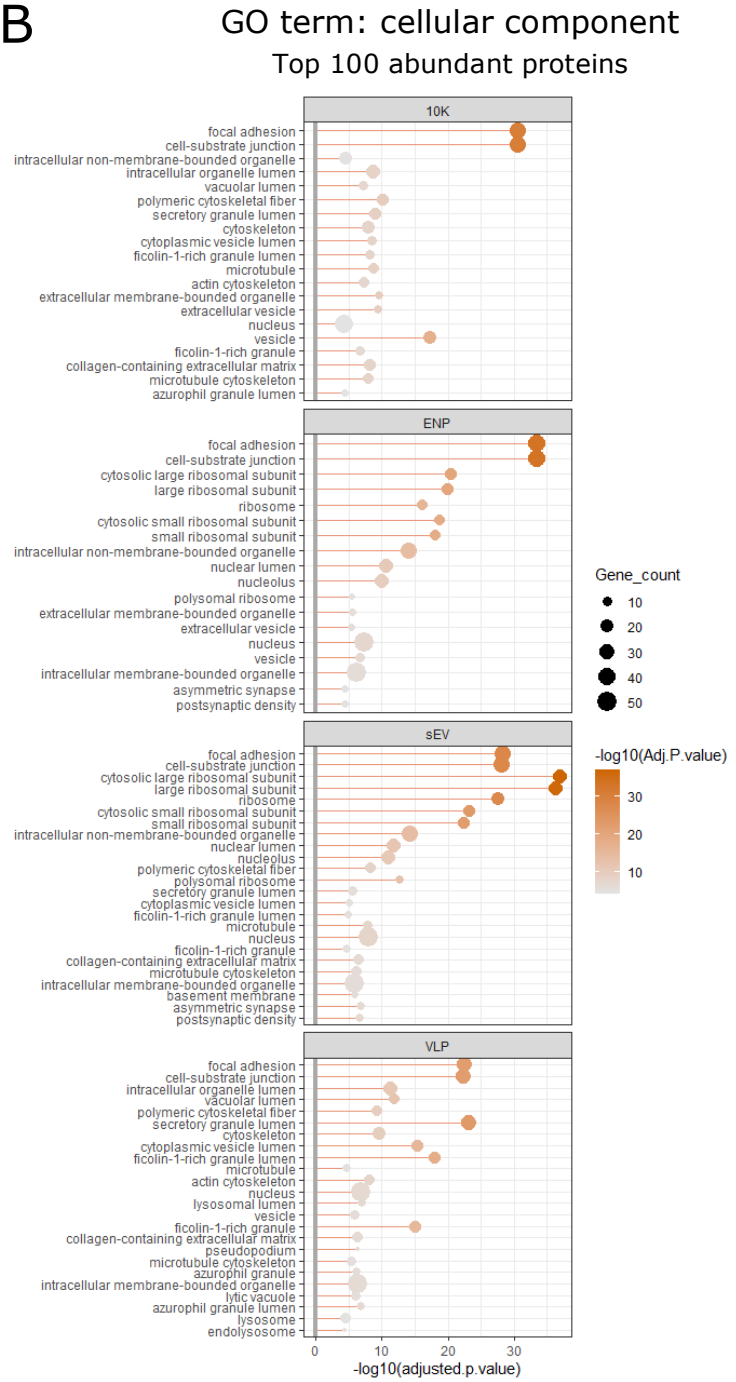

Threshold: p.value < 0,00001

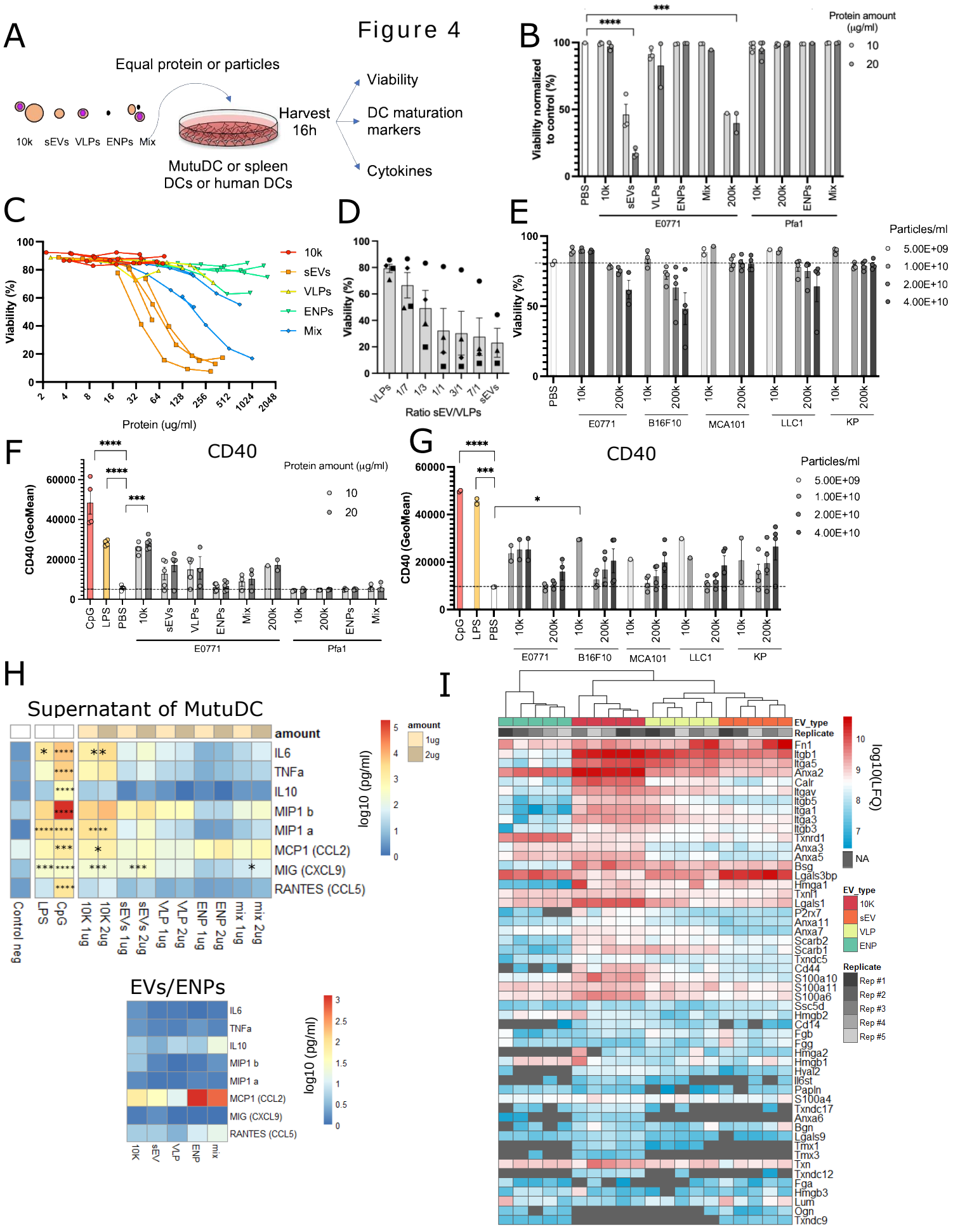
Figure 4
A
Equal protein or particles
10k sEVs VLPs ENPs Mix
MutuDC or spleen DCs or human DCs
Harvest 16h
Viability
DC maturation markers
Cytokines
B
Viability normalized to control (%)
Protein amount (µg/ml)
10
20
PBS 10k sEVs VLPs ENPs Mix 200k 10k 200k ENPs Mix
E0771
Pfa1
C
Viability (%)
Protein (ug/ml)
10k
sEVs
VLPs
ENPs
Mix
D
Viability (%)
VLPs 1/7 1/3 1/1 3/1 7/1 sEVs
Ratio sEV/VLPs
E
Viability (%)
Particles/ml
5.00E+09
1.00E+10
2.00E+10
4.00E+10
PBS 10k 200k 10k 200k 10k 200k 10k 200k 10k 200k
E0771 B16F10 MCA101 LLC1 KP
F
CD40
CD40 (GeoMean)
Protein amount (µg/ml)
10
20
CpG LPS PBS 10k sEVs VLPs ENPs Mix 200k 10k 200k ENPs Mix
E0771
Pfa1
G
CD40
CD40 (GeoMean)
Particles/ml
5.00E+09
1.00E+10
2.00E+10
4.00E+10
CpG LPS PBS 10k 200k 10k 200k 10k 200k 10k 200k 10k 200k
E0771 B16F10 MCA101 LLC1 KP
H
Supernatant of MutuDC
amount
IL6
TNFa
IL10
MIP1 b
MIP1 a
MCP1 (CCL2)
MIG (CXCL9)
RANTES (CCL5)
log10 (pg/ml)
amount
1ug
2ug
Control neg LPS CpG 10K 1ug 10K 2ug sEVs 1ug sEVs 2ug VLP 1ug VLP 2ug ENP 1ug ENP 2ug mix 1ug mix 2ug
EVs/ENPs
IL6
TNFa
IL10
MIP1 b
MIP1 a
MCP1 (CCL2)
MIG (CXCL9)
RANTES (CCL5)
log10 (pg/ml)
10K sEV VLP ENP mix
I
EV_type
Replicate
log10(FC)
NA
EV_type
10K
sEV
VLP
ENP
Replicate
Rep #1
Rep #2
Rep #3
Rep #4
Rep #5
Fn1 Itgb1 Itga5 Anxa2 Calr Itgav Itgb5 Itga1 Itga3 Itgb3 Txnrd1 Anxa3 Anxa5 Bsg Lgals3bp Hmga1 Txnl1 Lgals1 P2rx7 Anxa11 Anxa7 Scarb2 Scarb1 Txndc5 Cd44 S100a10 S100a11 S100a6 Ssc5d Hmgb2 Cd14 Fgb Fgg Hmga2 Hmgb1 Hyal2 Il6st Papln S100a4 Txndc17 Anxa6 Bgn Lgals9 Tmx1 Tmx3 Txn Txndc12 Fga Hmgb3 Lum Ogn Txndc9

Extended view 5

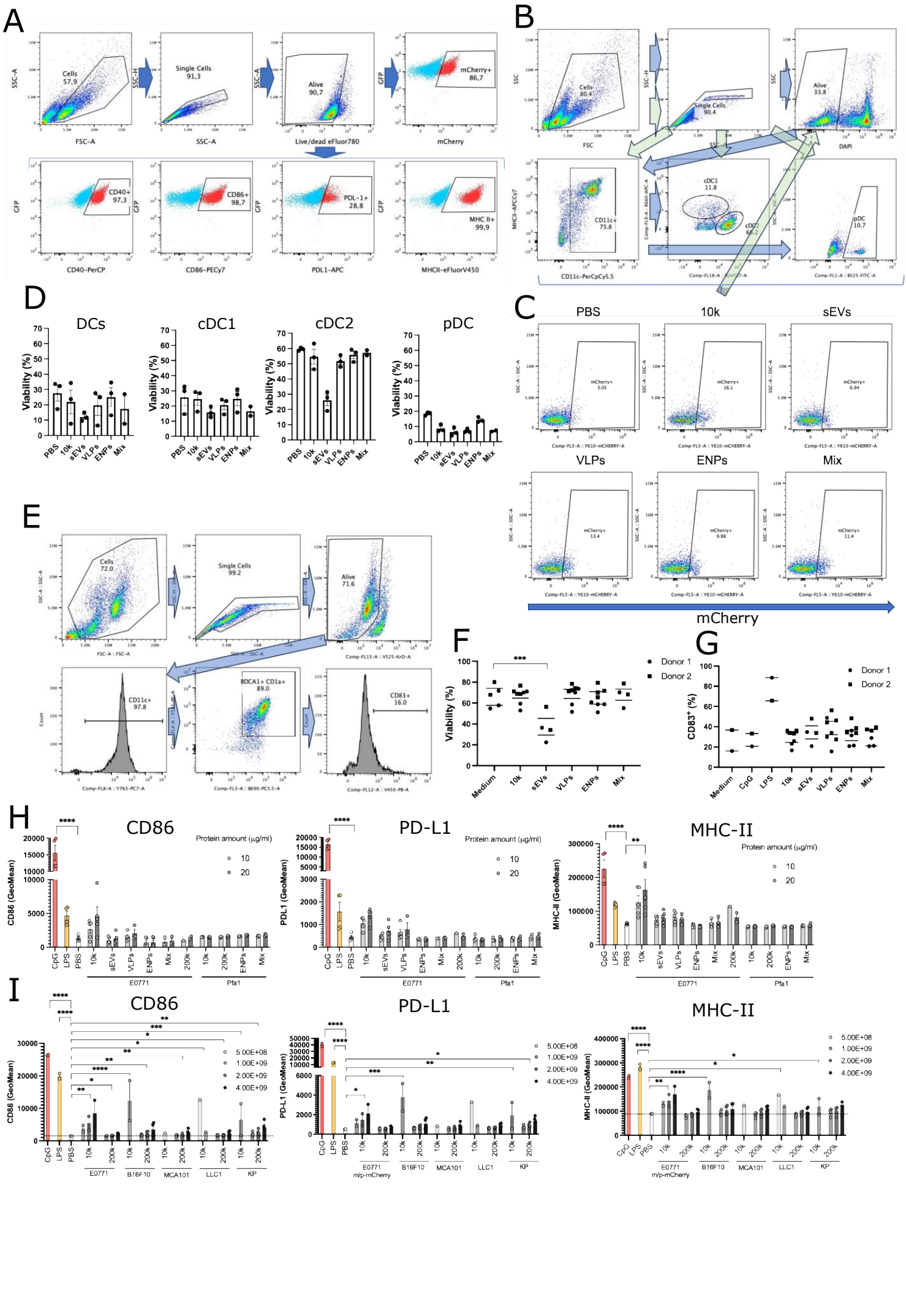

Figure 5

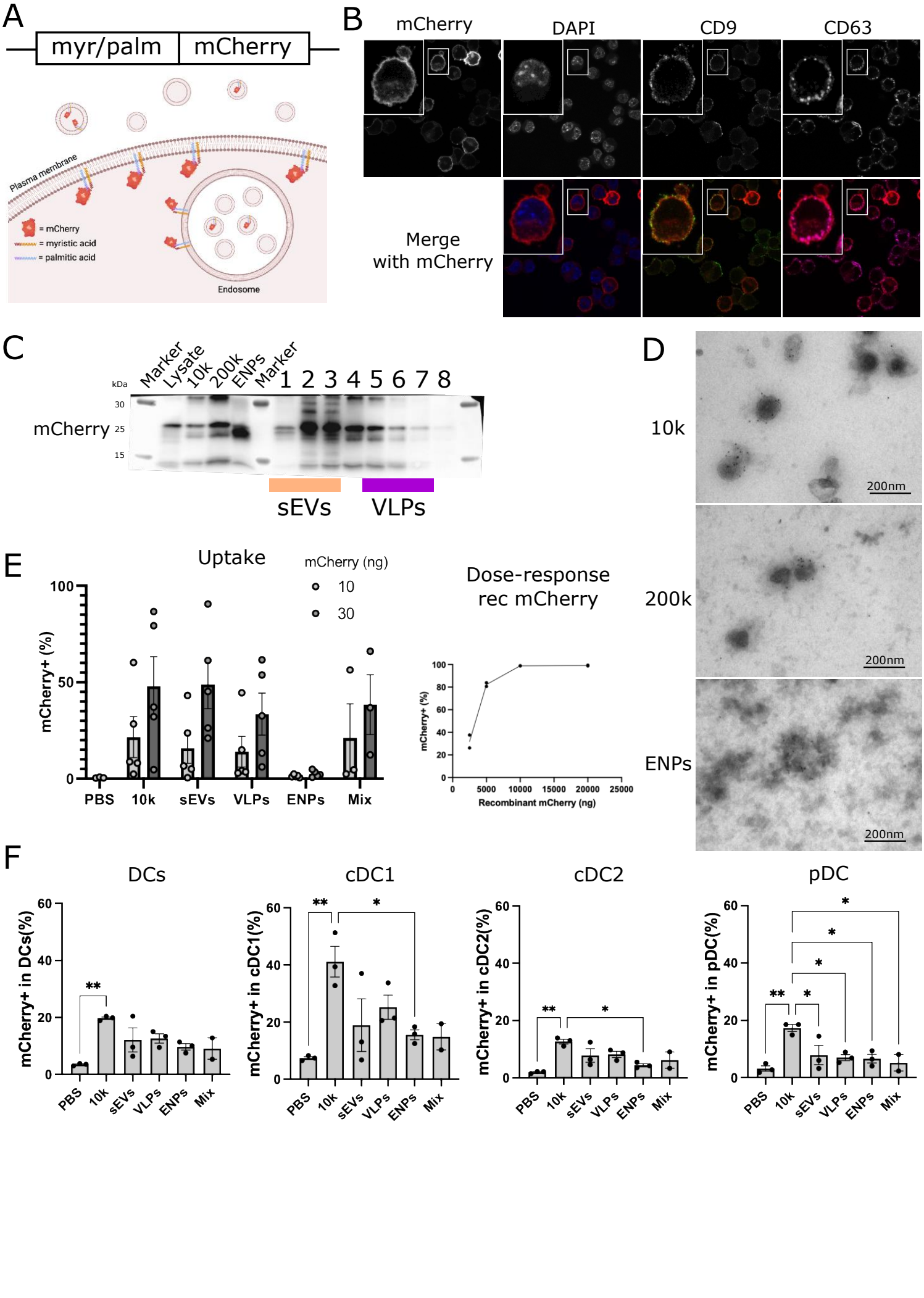
A
myr/palm
mCherry
Plasma membrane
= mCherry
= myristic acid
= palmitic acid
Endosome
B
mCherry
DAPI
CD9
CD63
Merge
with mCherry
C
Marker
Lysate
10k
200k
ENPs
Marker
1 2 3 4 5 6 7 8
kDa
30
25
15
mCherry
sEVs
VLPs
D
10k
200k
ENPs
200nm
E
Uptake
mCherry (ng)
10
30
mCherry+ (%)
PBS
10k
sEVs
VLPs
ENPs
Mix
Dose-response
rec mCherry
mCherry+ (%)
Recombinant mCherry (ng)
F
DCs
cDC1
cDC2
pDC
mCherry+ in DCs(%)
mCherry+ in cDC1(%)
mCherry+ in cDC2(%)
mCherry+ in pDC(%)

Extended view 6

A

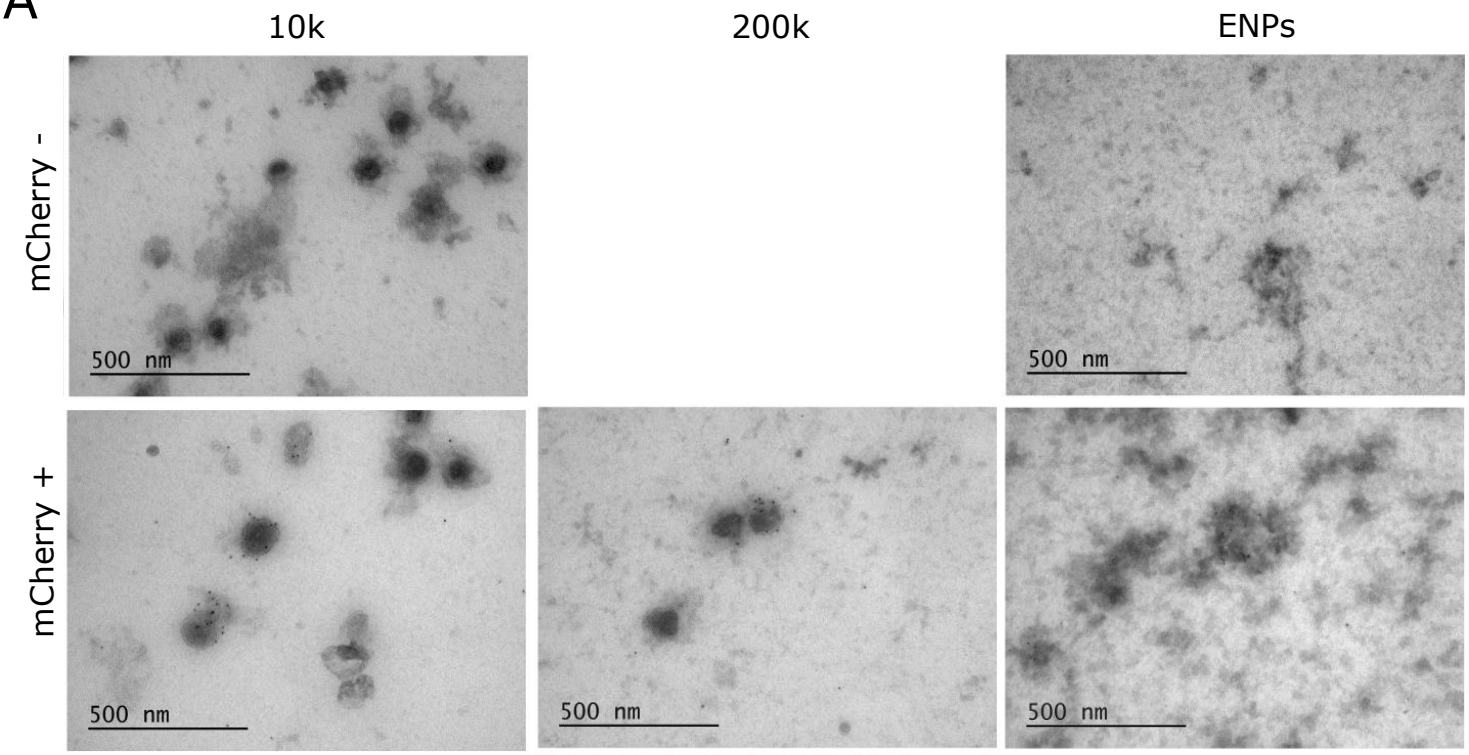

Figure 6

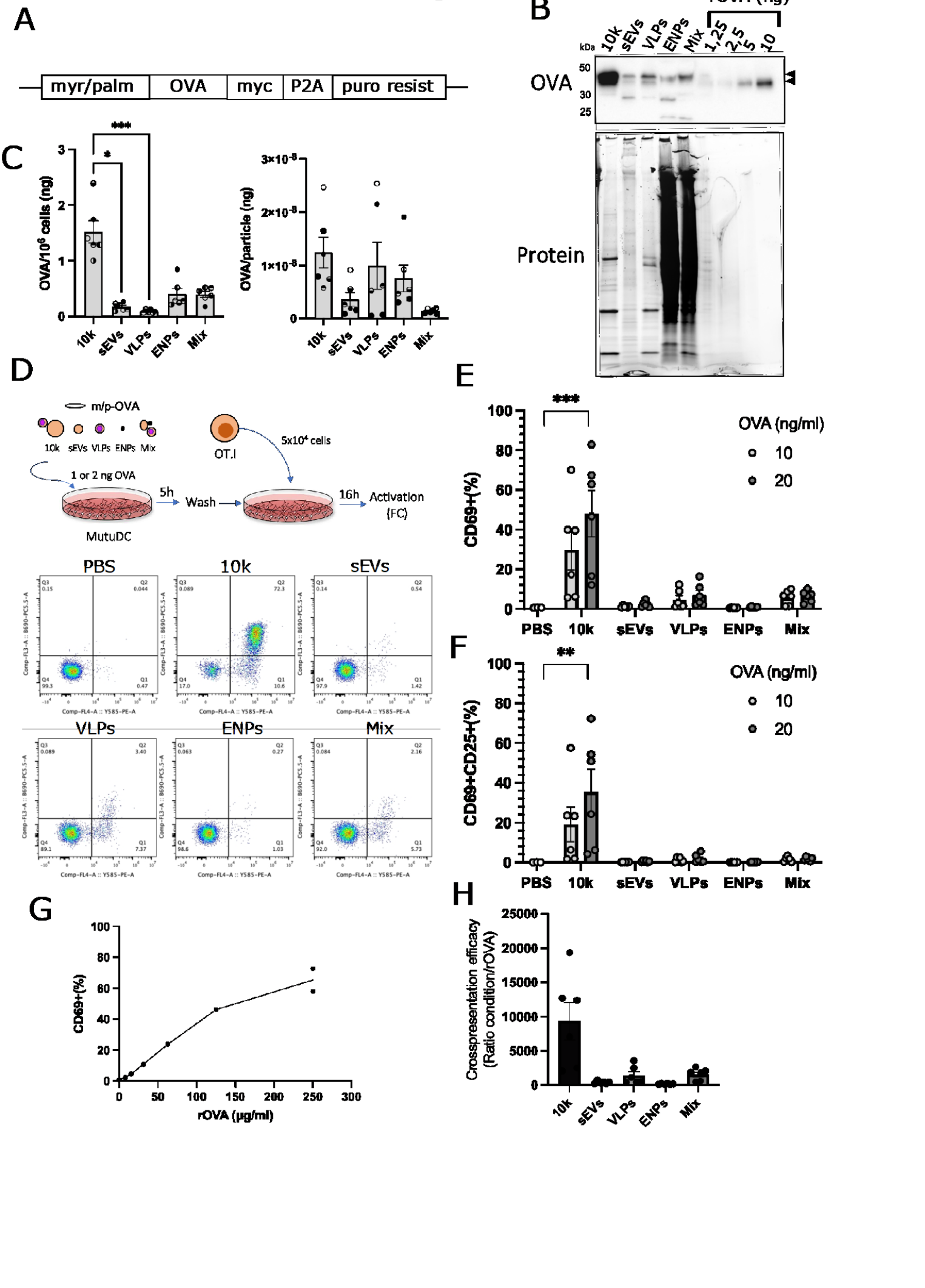
A
myr/palm
OVA
myc
P2A
puro resist
B
rOVA (ng)
kDa
10k
sEVs
VLPs
ENPs
Mix
1,25
2,5
5
10
50
30
25
OVA
Protein
C
OVA/10^6 cells (ng)
OVA/particle (ng)
10k
sEVs
VLPs
ENPs
Mix
D
m/p-OVA
10k sEVs VLPs ENPs Mix
OT.I
5x10^4 cells
1 or 2 ng OVA
5h
Wash
16h
Activation (FC)
MutuDC
PBS
10k
sEVs
VLPs
ENPs
Mix
E
CD69+(%)
OVA (ng/ml)
10
20
F
CD69+CD25+(%)
G
CD69+(%)
rOVA (µg/ml)
H
Crosspresentation efficacy (Ratio condition/rOVA)

ABSTRACT

Cells secrete extracellular vesicles (EVs) and non-vesicular extracellular (nano)particles (NVEPs or ENPs) that may play a role in intercellular communication. Tumor-derived EVs have been proposed to induce immune priming of antigen presenting cells, or to be immuno-suppressive agents. We suspect that such disparate functions are due to variable compositions in EV subtypes and ENPs. We aimed to characterize the array of secreted EVs and ENPs of murine tumor cell lines. Unexpectedly, we identified virus-like particles (VLPs) from endogenous murine leukemia virus in preparations of EVs produced by many tumor cells. We established a protocol to separate small (s)EVs from VLPs and ENPs. We compared their protein composition and analyzed their functional interaction with target dendritic cells (DCs). ENPs were poorly captured and did not affect DCs. sEVs specifically induced DC death. A mixed large EV/VLP preparation was most efficient to induce DC maturation and antigen presentation. Our results call for systematic re-evaluation of the respective proportions and functions of non-viral EVs and VLPs produced by tumors and their contribution to tumor progression.

Keywords:
antigen presenting cells / exosomes / extracellular vesicles / non vesicular extracellular particles / retrovirus / tumors.

Figures to be downloaded:
http://xfer.curie.fr/get/qUNIhiMe2YR/All%20figures%20revision%20230829.pptx

Extracellular vesicles and co-isolated endogenous retroviruses differently affect dendritic cells

Federico Cocozza[1,2], Lorena Martin-Jaular[1,3], Lien Lippens[4], Aurelie Di Cicco[5,6], Yago A Arribas[1], Nicolas Ansart[1], Florent Dingli[7], Michael Richard[7], Louise Merle[1], Mabel Jouve[8], Patrick Poullet[9], Damarys Loew[7], Daniel Lévy[5,6], An Hendrix[4], George Kassiotis[10], Alain Joliot[1], Mercedes Tkach[1]*, Clotilde Théry[1,3]*

[1]INSERM U932, Institut Curie Centre de Recherche, PSL Research University, F-75005, Paris, France
[2]Université de Paris, F-75006, Paris, France
[3]Institut Curie centre de recherche, CurieCoreTech Extracellular Vesicles, F-75005, Paris, France
[4]Laboratory of Experimental Cancer Research, Ghent University, Ghent, Belgium
[5]Institut Curie, PSL Research University, Sorbonne Université, CNRS UMR168, Laboratoire Physico-chimie Curie, F-75005, Paris, France
[6]Institut Curie, PSL Research University, CNRS UMR144, Cell and Tissue Imaging Facility (PICT-IBiSA), F-75005, Paris, France
[7]Institut Curie, PSL Research University, Centre de Recherche, CurieCoreTech Spectrométrie de Masse Protéomique, F-75005, Paris, France
[8]CNRS UMR3215, Institut Curie, PSL Research University, F-75005, Paris, France
[9]Institut Curie, Bioinformatics core facility (CUBIC), INSERM U900, PSL Research University, Mines Paris Tech, F-75005, Paris, France
[10]Retroviral Immunology, The Francis Crick Institute and Department of Medicine, Faculty of Medicine, Imperial College, London UK

*co-last authors.
Correspondence to: clotilde.thery@curie.fr. ORCID 0000-0001-8294-6884
mercedes.tkach@gmail.com. ORCID 0000-0002-8011-9444

Total character count: 91215 (w space, w/o figure legends)